

AD-A084 903

NAVAL POSTGRADUATE SCHOOL MONTEREY CA
A MODEL FOR LASER PRODUCED MATERIAL SURFACE EVAPORATION. (U)
MAR 80 G L TRAVERS

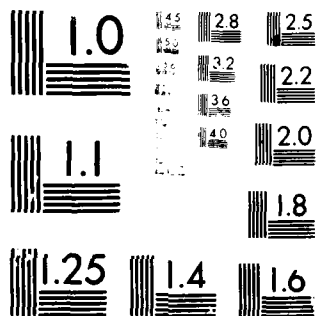
F/6 20/5

UNCLASSIFIED

NL

1 of 1
AD
A084903

END
DATE
FILMED
6-80
DTIC



MICROCOPY RESOLUTION TEST CHART
NATIONAL BUREAU OF STANDARDS-1963-A

LEVEL II

2

NAVAL POSTGRADUATE SCHOOL

Monterey, California

ADA 084903



DTIC
ELECTE
JUN 2 1980
S D C

9) Masters **THESIS**

6 A MODEL FOR LASER PRODUCED MATERIAL SURFACE EVAPORATION.

by

40 Geoffrey Lance Travers

11 Mar 1980 12 73

Thesis Advisor: K.E. Woehler

Approved for public release; distribution unlimited.

DC FILE COPY

80 5 30 0 62

REPORT DOCUMENTATION PAGE		READ INSTRUCTIONS BEFORE COMPLETING FORM	
1. REPORT NUMBER	2. GOVT ACCESSION NO. AD-A084 903	3. RECIPIENT'S CATALOG NUMBER	
4. TITLE (and Subtitle) A Model for Laser Produced Material Surface Evaporation		5. TYPE OF REPORT & PERIOD COVERED Master's Thesis; March 1980	6. PERFORMING ORG. REPORT NUMBER
7. AUTHOR(s) Geoffrey Lance Travers		8. CONTRACT OR GRANT NUMBER(s)	
9. PERFORMING ORGANIZATION NAME AND ADDRESS Naval Postgraduate School Monterey, California 93940		10. PROGRAM ELEMENT, PROJECT, TASK AREA & WORK UNIT NUMBERS	
11. CONTROLLING OFFICE NAME AND ADDRESS Naval Postgraduate School Monterey, California 93940		12. REPORT DATE March 1980	
		13. NUMBER OF PAGES 72	
14. MONITORING AGENCY NAME & ADDRESS (if different from Controlling Office)		15. SECURITY CLASS. (of this report) Unclassified	
		15a. DECLASSIFICATION/DOWNGRADING SCHEDULE	
16. DISTRIBUTION STATEMENT (of this Report) Approved for public release; distribution unlimited.			
17. DISTRIBUTION STATEMENT (of the abstract entered in Block 20, if different from Report)			
18. SUPPLEMENTARY NOTES			
19. KEY WORDS (Continue on reverse side if necessary and identify by block number) Laser Radiation Adiabatic jet expansion model			
20. ABSTRACT (Continue on reverse side if necessary and identify by block number) → This study is to assess the feasibility of using a laser's radiation to remove masses on the order of milligrams from a target surface and to form a vapor jet which could then serve as the conducting channel in a giant power pulse discharge. A model based on an energy balance is presented which predicts the mass removed and the pressure, density and temperature of the material as it propagates from the target surface as functions of the pulse time →			

#20 - ABSTRACT - Continued

→ and the absorbed power density. Combinations of laser pulse time and power density are considered for which the surface temperature remains low enough in order to avoid cut-off by a plasma plume in front of the target surface.

A model of adiabatic jet expansion is presented to predict the radial expansion of the vapor plume as it propagates in the axial direction. Temperature, pressure and density are predicted after radial expansion using the model of adiabatic jet expansion.

These models predict, theoretically, that the desired masses and limits on vapor plume expansion can be achieved using relatively low power densities for the proposed experiment. ←

Accession For	
NTIS GRA&I	<input checked="" type="checkbox"/>
DDC TAB	<input type="checkbox"/>
Unannounced	
Justification	
By _____	
Distribution/	
Availability Codes	
Dist	Avail and/or special
A	

Approved for public release; distribution unlimited.

A Model for Laser Produced Material
Surface Evaporation

by

Geoffrey Lance Travers
Lieutenant, United States Navy
B.S., University of Missouri, 1974

Submitted in partial fulfillment of the
requirements for the degree of

MASTER OF SCIENCE IN PHYSICS

from the

NAVAL POSTGRADUATE SCHOOL

March 1980

Author

Geoffrey L. Travers

Approved by:

W. F. Walker

Thesis Advisor

F. Schmirer

Second Reader

J. M. Dyer

Chairman, Department of Physics and Chemistry

William M. Tolles

Dean of Science and Engineering

ABSTRACT

This study is to assess the feasibility of using a laser's radiation to remove masses on the order of milligrams from a target surface and to form a vapor jet which could then serve as the conducting channel in a giant power pulse discharge.

A model based on an energy balance is presented which predicts the mass removed and the pressure, density and temperature of the material as it propagates from the target surface as functions of the pulse time and the absorbed power density. Combinations of laser pulse time and power density are considered for which the surface temperature remains low enough in order to avoid cut-off by a plasma plume in front of the target surface.

A model of adiabatic jet expansion is presented to predict the radial expansion of the vapor plume as it propagates in the axial direction. Temperature, pressure and density are predicted after radial expansion using the model of adiabatic jet expansion.

These models predict, theoretically, that the desired masses and limits on vapor plume expansion can be achieved using relatively low power densities for the proposed experiment.

TABLE OF CONTENTS

I.	INTRODUCTION -----	6
II.	THE ABSORPTION PROCESS -----	12
III.	THERMAL RESPONSES -----	23
	A. THE MODEL -----	23
	B. THE THEORY OF EVAPORATION -----	31
	1. Assumptions -----	31
	2. Temperature Profile in the Material --	32
	3. Energy Balance -----	32
	4. The Mass Removed -----	37
	5. Axial Expansion of the Vapor Jet -----	37
	6. Density and Pressure in the Plume ----	40
	7. Limits on T_g to Avoid Ionization ----	42
IV.	RADIAL EXPANSION OF THE VAPOR PLUME -----	45
V.	RESULTS -----	51
	A. CASE I. SMALL PULSE TIMES -----	51
	B. CASE II. LONG PULSE TIMES -----	53
	C. MASS REMOVAL CALCULATION -----	53
VI.	CONCLUSION -----	60
	APPENDIX A -----	62
	BIBLIOGRAPHY -----	70
	INITIAL DISTRIBUTION LIST -----	72

I. INTRODUCTION

Requirements for material and equipment tests at very high x-ray radiation fluxes with particular spectral characteristics have led to the development of giant pulse power devices, Johnson [1].

The technique of using "exploding wires" or wire arrays dates back to 1773 [2]. In this technique the energy from a large storage capacitor is discharged first through a pulse forming network then through thin metallic wires which pinch due to the development of large magnetic fields and eventually develop into a high temperature plasma which becomes a source of high intensity x-rays. In recent time the wire array has been replaced by a gas-puff from a supersonic nozzle. After preionization with microwave radiation the discharge through the gas jet leads to a high temperature pinch discharge.

The x-ray intensity and spectral distribution depends upon the high voltage pulse form, plasma temperature and dynamics, mass of the wire array or gas in the gas-puff, z-number of the material and the overall geometry of the experiment. Elaborate computer codes, Colombant [3], have been written to model the x-ray emission as a function of these parameters. In order to obtain the desired spectra and intensities, these computer codes predict masses on the order of milligrams and high z-number materials are required in the discharge channel.

Wire arrays are not available in small enough diameter sizes for high z-number materials. As for the gas-puff device, materials again are severely limited to gaseous elements such as Ar, Kr, and Xe. Because of the shortcomings of wire arrays to satisfy the mass and z-number requirements, alternate methods of establishing high energy discharge channels are of interest.

The use of high power laser pulses directed at a target material has been proposed by Schwirzke, described by Johnson [1]. In such a scheme, the target material in the form of a solid disc can be mounted on the anode (or cathode) of a high voltage pulsed power machine. A laser beam is directed toward the target and a certain mass of the target is vaporized, figure 1. This vapor plume will expand through the evacuated chamber toward the cathode. Electrical energy would then couple to the vapor plume producing a pinched discharge channel with an intense x-ray emission. Preionization of the vapor could be done by microwaves as in the gas-puff experiment or conceivably by the laser itself. The advantages of this concept over wire arrays and gas-puffs are great in principle as targets could conceivably be made of almost any material.

By controlling the energy, pulse width and focal area of the laser along with the choice of material, the x-ray emission spectrum could be varied. Combinations of different materials could also be used.

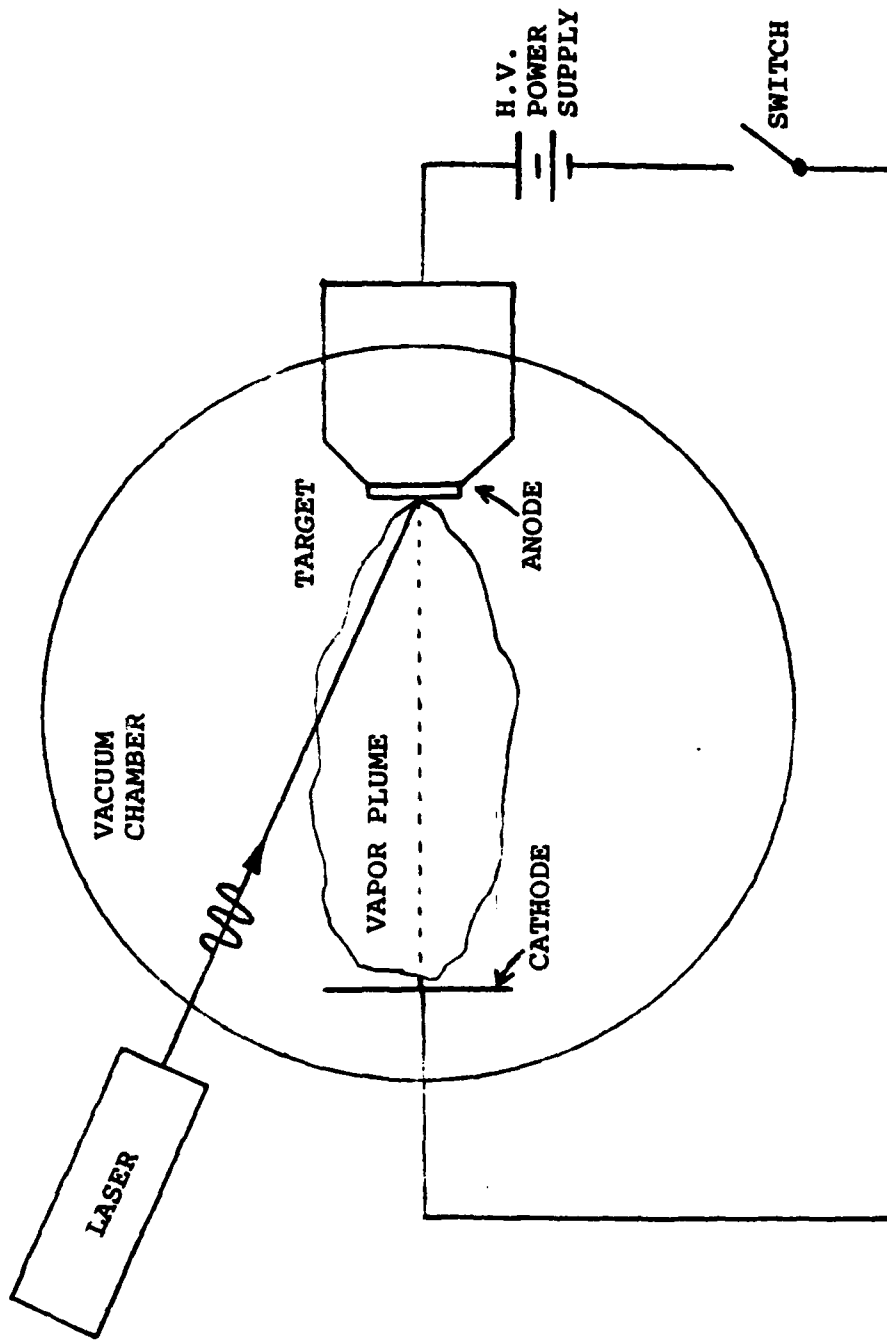


FIGURE 1. ILLUSTRATING THE PROPOSED EXPERIMENT

There are two distinct mechanisms by which a laser can remove material from a target. First, the laser energy is absorbed by the target to increase the temperature to the vaporization temperature. At high power densities this takes a very short time, on the order of a few nanoseconds. Since the power density is large, a high percentage of ionization in the vapor cloud or plume will be reached after a very short time. This high ionization level causes absorption of the laser energy in the plume thus shielding the target surface from the continuing incoming radiation. However, further vaporization of the surface via electronic heat conduction continues. This mechanism has been investigated by Brooks [4]. He used a Q-switched neodymium glass laser with a 5 Joule output of pulse duration 25 nsec directed at an aluminum target with a focal diameter of 0.15 cm. This results in a power density of about 10^{10} Watts/cm². Measurements showed mass removal to be about 0.7 mg. While the mass yield is of the desired order, an important feature of this mechanism makes it less attractive for the purpose here. The main plasma, carrying the bulk of the ionized mass, propagated at 1.1×10^7 cm/sec. If anode-cathode separation were assumed to be 4 cm, the main plasma would reach the anode in 364 nsec. The target temperature is so high that vaporization continues for almost 10 μ sec after the laser pulse is stopped. As a result, the plasma particles in the plume will expand, thus filling the entire cavity before sufficient mass has been removed from the target. As the plasma now covers a large volume, energy

coupling from the high voltage source will become difficult. Contamination of and arcing in the gap of the coaxial delay line forming the cathode cone will reduce efficiency.

An alternate approach may be used to overcome this problem. If the laser power density is lowered the ionization level can be reduced to a point where no significant absorption of the laser's radiation takes place in the vapor plume. This plume is now a true vapor plume and not a plasma. The laser energy is not shielded from the target surface. As the surface temperature is now relatively low, the plume propagates much slower. The timing of the application of the high voltage can be made to correspond to the travel time of the vapor plume. The question is whether significant masses, on the order of milligrams, can be removed from the target. This is the approach that will be studied in this paper.

There are many parameters controlling the mass removal process. The energy delivered by the laser to the material surface divides into the reflected portion and the absorbed portion. Classically the absorption is dependent on the laser radiation wavelength and the conductivity of the target material. In section II, the relevant absorption processes are described for various materials of interest and a table of absorption is compiled which is used as the basis for the absorption calculated.

The absorbed energy at the surface raises the temperature of the material leading eventually to melting and vaporization beginning at the surface. The initially steep temperature

gradient near the surface leads to rapid heat conduction into the material. This process is governed by the heat conduction equation. Because of the three phases present this is a very complex problem. There are many models of this process using various approximations in the literature, often employing elaborate computer programs. In order to stay with the purpose of this study, to assess the general feasibility of the proposed mechanism, a very simple model of the heat conduction and evaporation has been adopted which will be discussed in Section III. Its relation to other models in the literature are also discussed.

As the material evaporates from the surface it expands both axially and radially. Section IV deals with the radial expansion which is described as an adiabatic jet expansion. Density, temperature and pressure changes in the expansion process are also described.

II. THE ABSORPTION PROCESS

Materials can be divided into three basic classes, conductors, semi-conductors and dielectrics. Dielectric materials are not of interest here because they do not conduct well. In order to vaporize these materials, high power densities must be used which would result in plasma production at the target surface. This is a condition we are trying to avoid as these high temperature plasmas lead to surface shielding.

Semi-conducting materials in general are also poor conductors. However, at certain wavelengths, there are resonances where conduction is quite high. In these regions their thermal properties resemble those of metals. Therefore, our considerations will be confined to the metallic absorption process.

The interaction of materials with electromagnetic waves is formulated on the basis of Maxwell's equations. This development is well known and documented [5, 6, 7]. Derivation of optical quantities is presented in Appendix A.

Plots can be made of absorbtivity, A vs. λ , the wavelength, for several materials using the following expression:

$$A = \frac{4n}{(n+1)^2 + k^2} \quad (\text{eq. 2-1})$$

where n and k are the real and imaginary parts of the complex index of refraction. The n and k are both functions of

frequency, ω , the conductivity, σ , and the parameter m^*/N where m^* is the effective mass and N is the free electron density of the metal. In general it is very difficult to obtain an appropriate value for m^* . Much controversy has arisen on how to measure effective mass, Seitz [8] lists some approximate values which are shown in Table 1. Harrison and Webb [9] review analytical and experimental work which illustrates the difficulty in obtaining appropriate values. This problem of choosing a value for m^* need not present an obstacle, however. Wieting and Schriempf [7] show proof that the sensitivity of reflectivity to the parameter β/N , where $\beta = m^*/m_0$, is small. Here m_0 is the free electron mass. Therefore, the selection of values for m^* in [8] are justified for our purpose.

Figures 2-9 are plots of n , k , and A as functions of decreasing wavelength using the data from Table I. It is interesting that the values for absorbtivity are very low for the region where ω is smaller than the plasma frequency. The absorbtivity then increases very sharply at the plasma frequency for the electrons in the metal and quickly reaches 100 percent. The degree of absorption remains relatively constant over the infrared region and is small, generally 1-2 percent.

The question now arises as to whether the calculated values for absorbtivity are reasonable. Bennett, Silver and Ashley [10] have shown surprisingly close correlations between experiment and these classically calculated absorbtivities in

TABLE I

MATERIAL	CONDUCTANCE $\text{ohms}^{-1} \text{m}^{-1}$	COEFFICIENT RESISTIVITY $\text{ohms}^{-1} \text{m}^{-1}$ T^{-1}	m^*/m	FREE ELECTRONS PER ATOM	FREE ELECTRON DENSITY m^{-3}
	*	*	**	***	
Al	3.77×10^7	4.3×10^{-11}	1.61	3.5	2.11×10^{29}
Ag	6.29×10^7	4.1×10^{-11}	1.07	1.3	7.62×10^{28}
Cd	1.46×10^7	4.2×10^{-11}	1.3	2.5	1.15×10^{29}
Zn	1.69×10^7	4.2×10^{-11}	1.3	2.9	1.91×10^{29}

*CRC Handbook [11].

**Seitz [8].

***Richtmyer, Kennard, Cooper [12].

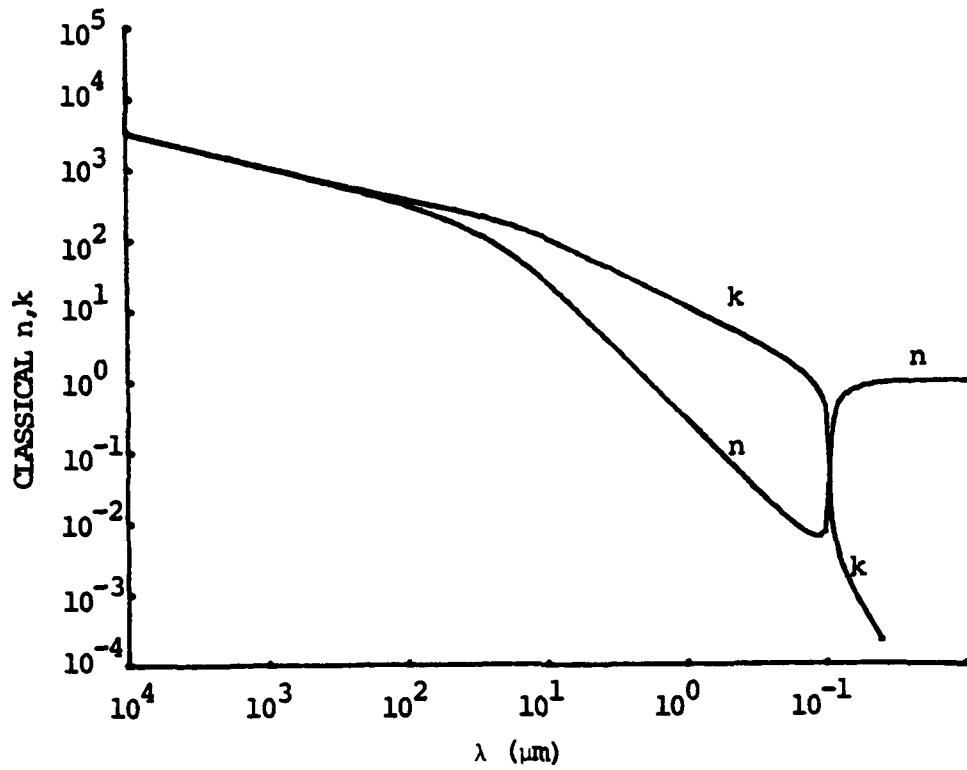


FIGURE 2. n, k vs. DECREASING WAVELENGTH FOR ALUMINUM

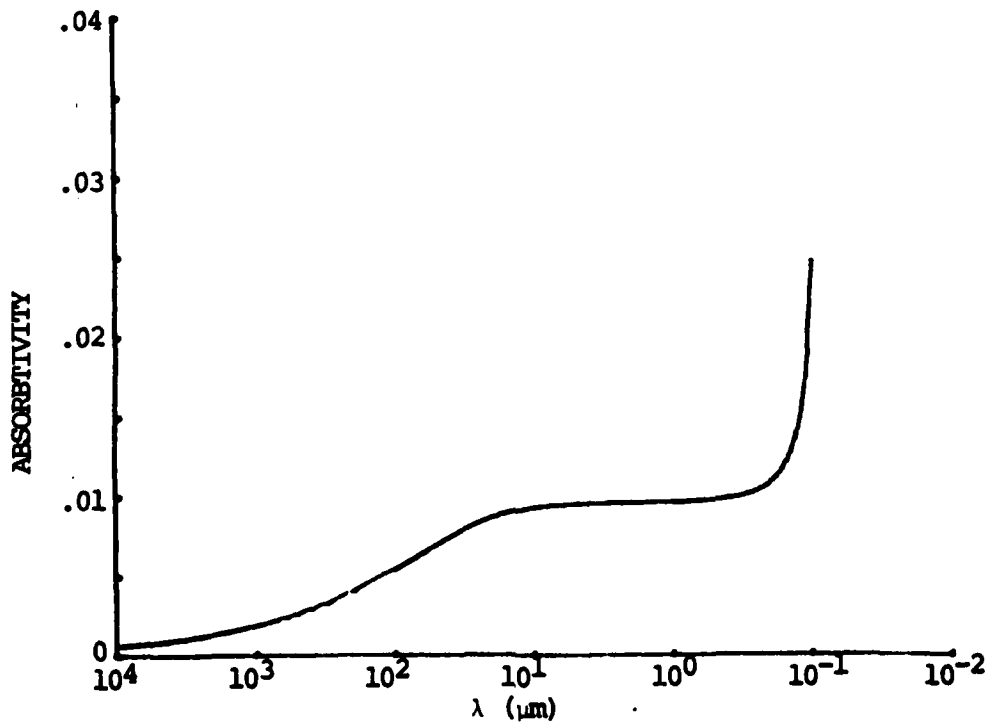


FIGURE 3. ABSORPTIVITY vs. DECREASING WAVELENGTH FOR ALUMINUM

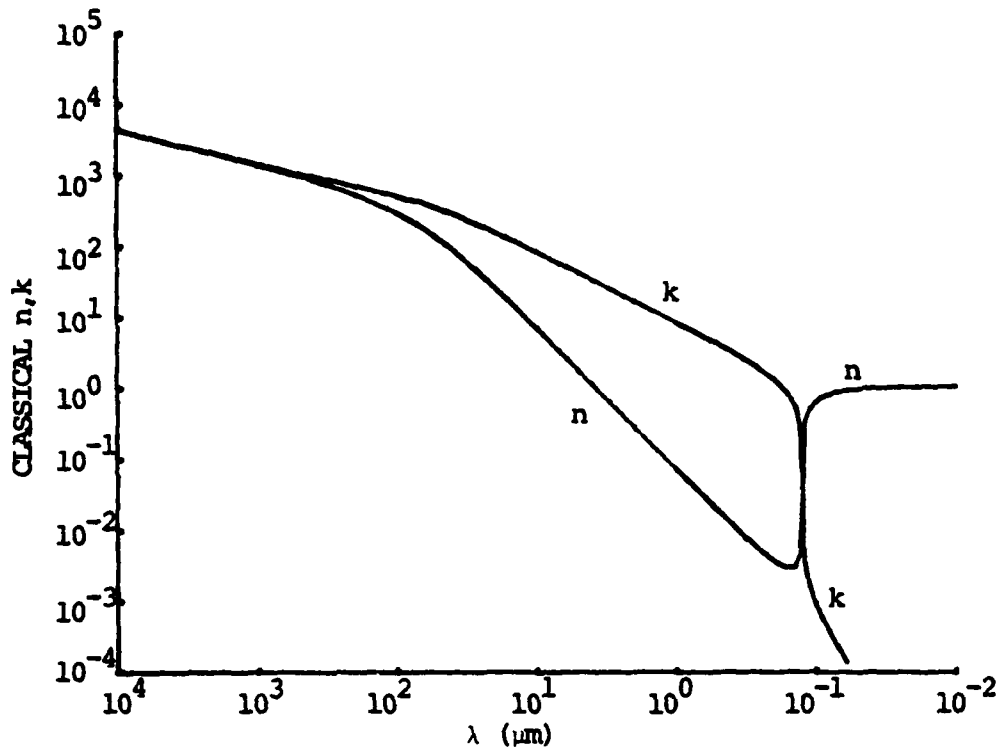


FIGURE 4. n, k vs. DECREASING WAVELENGTH FOR SILVER

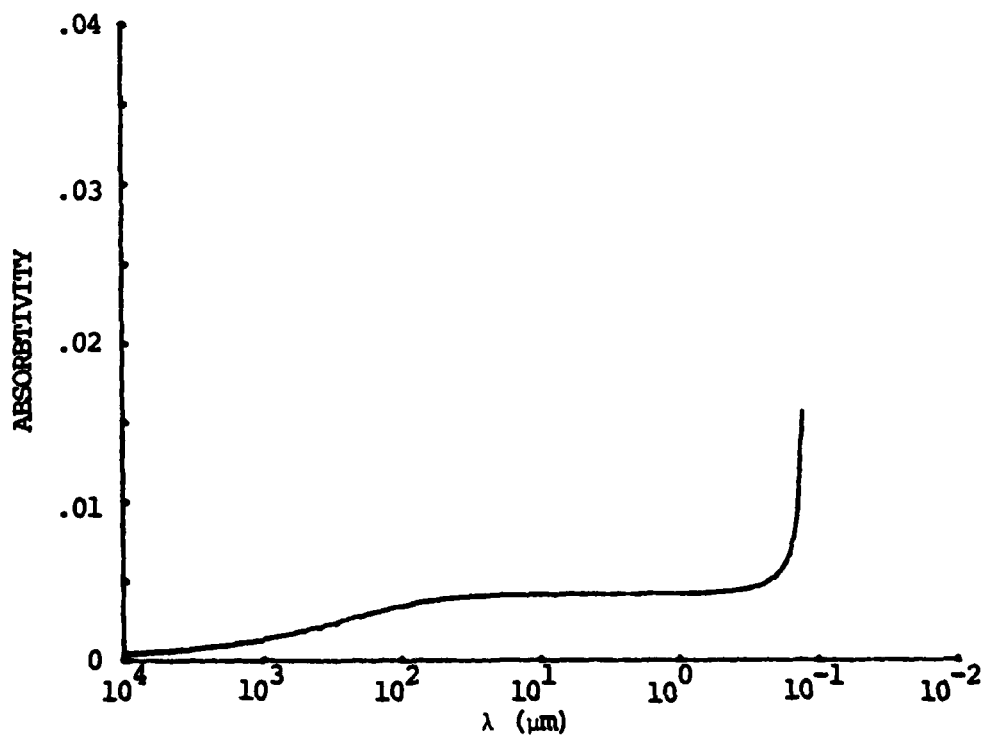


FIGURE 5. ABSORBTIVITY vs. DECREASING WAVELENGTH FOR SILVER

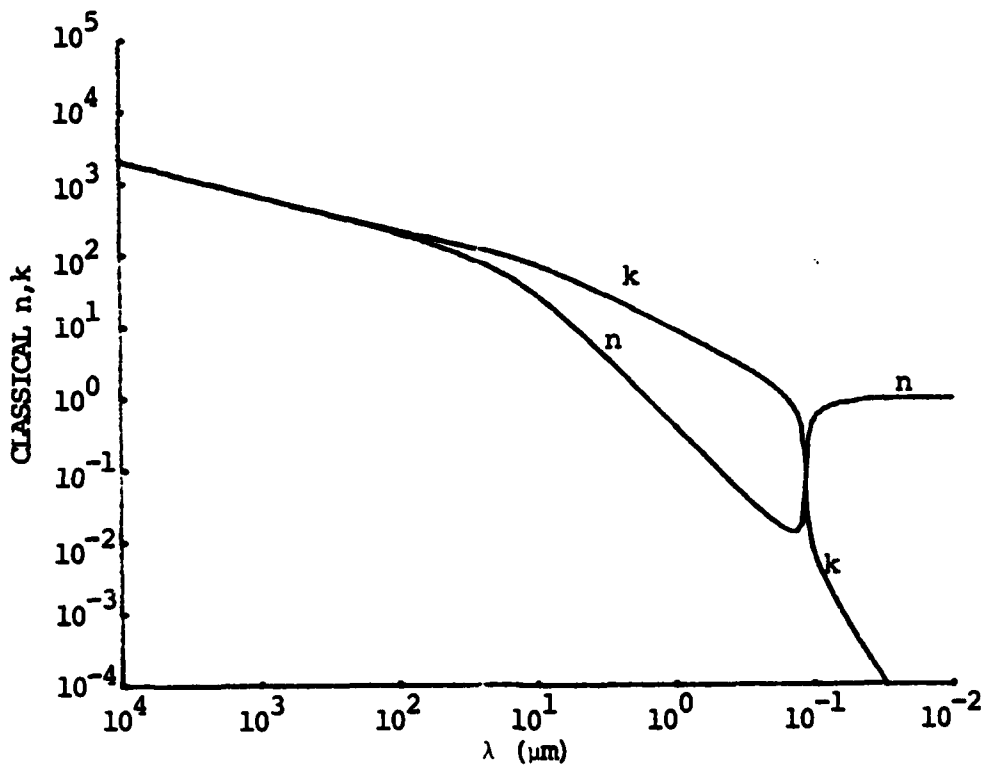


FIGURE 6. n, k vs. DECREASING WAVELENGTH FOR CADMIUM

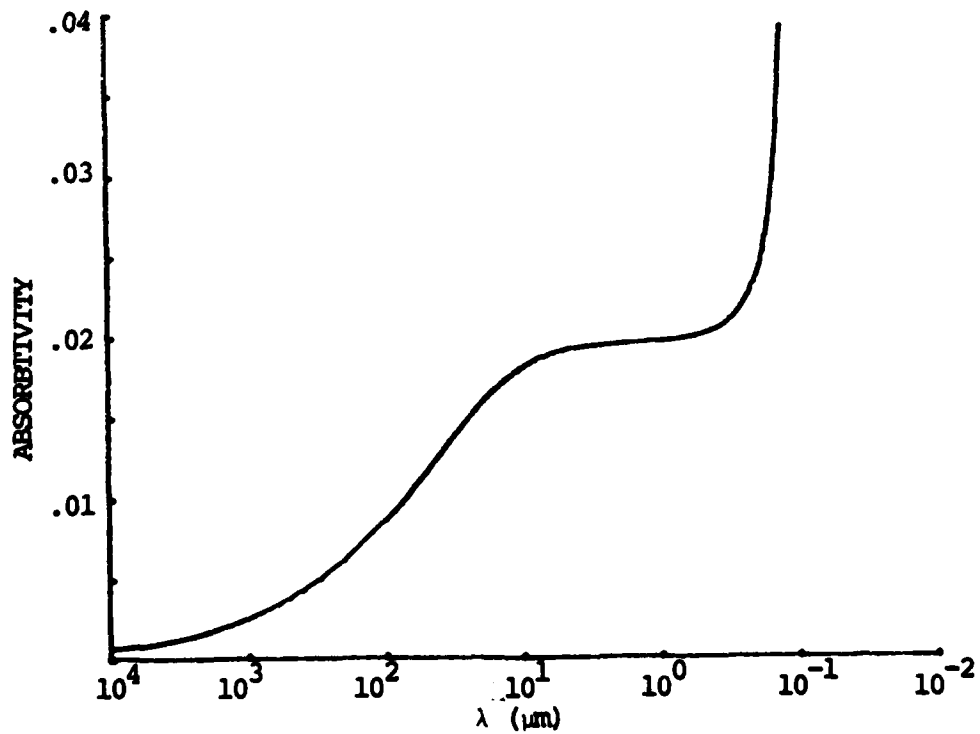


FIGURE 7. ABSORPTIVITY vs. DECREASING WAVELENGTH FOR CADMIUM

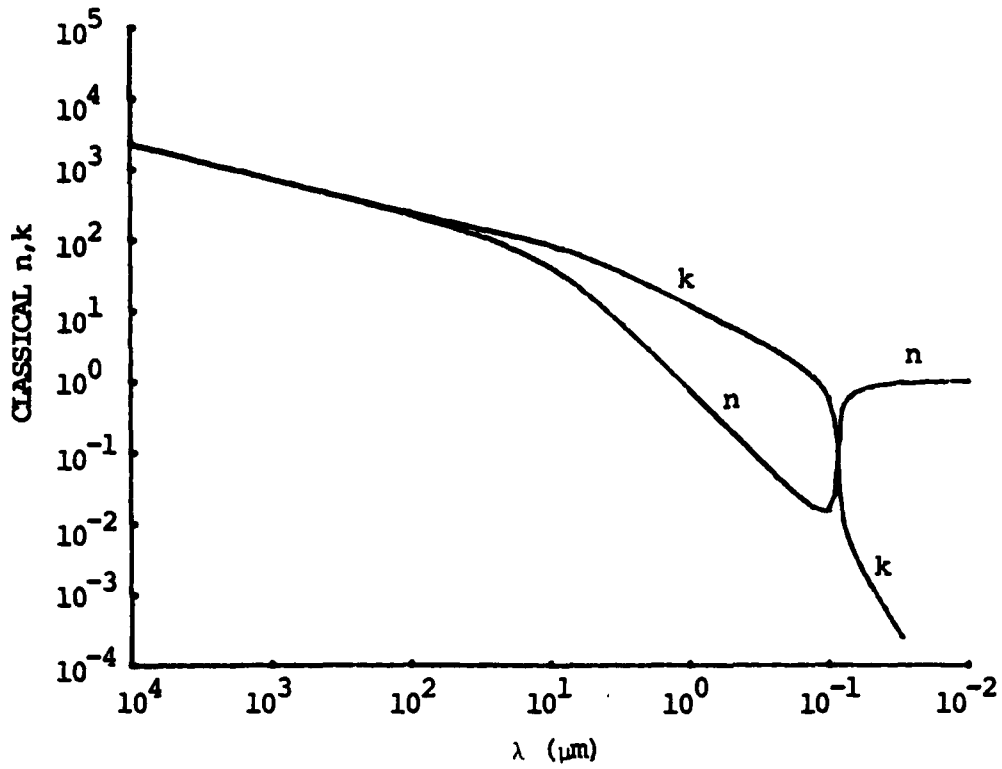


FIGURE 8. n, k vs. DECREASING WAVELENGTH FOR ZINC

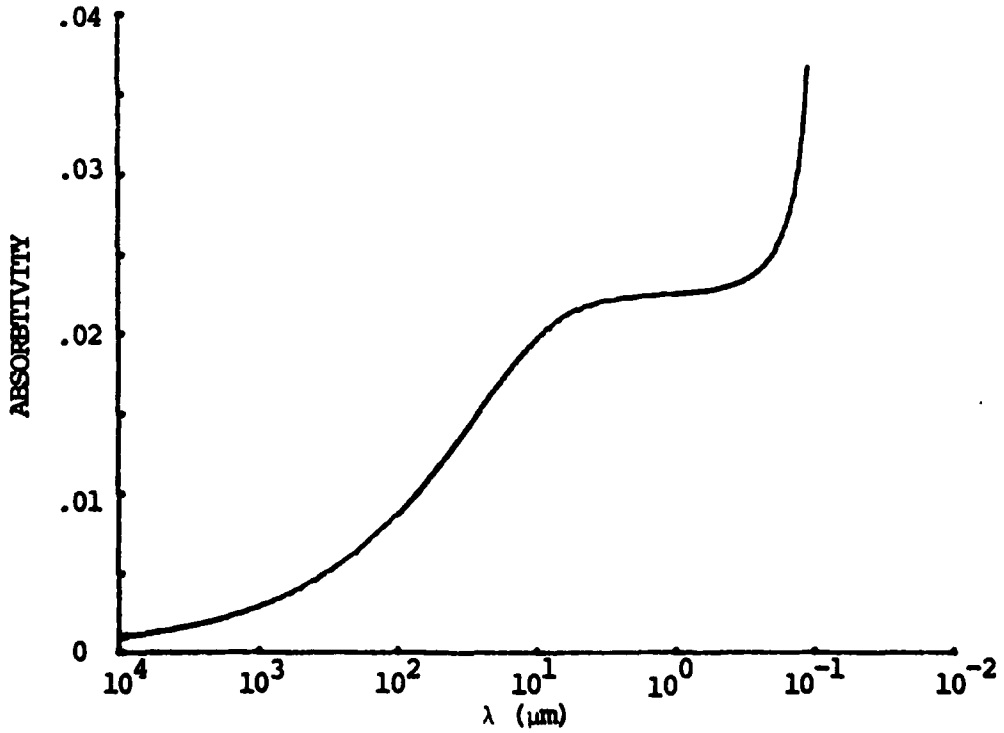


FIGURE 9. ABSORPTIVITY vs. DECREASING WAVELENGTH FOR ZINC

ultra high vacuums of 10^{-10} torr for aluminum. However, at lower values of vacuum the theory breaks down and the absorbtivity is greater. This is significant because in this experiment the base pressure in the vacuum chamber is 10^{-4} torr. Bonch-Bruevich [13] also shows experimental results illustrating the change in reflectivity as a function of pulse time in copper and steel, figure 10. It must be pointed out, however, that these results pertain to conditions different from those of interest here. This particular experiment was carried out using a laser with a power density on the order of 10^{10} Watts/cm². At this high power level there may be major plasma production and the marked decrease in reflectivity at the target surface is probably due more to the plume absorption rather than the temperature dependent changing of optical properties of the target material. The first plateau at 2 μ sec is probably due to the onset of vaporization. One would not expect a much lower power level laser to produce the degree of change in absorbtivity that Bonch-Bruevich observed.

In calculating the absorbtivity, dc conductivity was used. Conductivity is inversely proportional to the resistivity. The resistivity of metals increases nearly linearly with temperature in the region from room temperature to melting. Figure 11 is a plot of absorbtivity as a function of temperature for four metals, aluminum, silver, cadmium and zinc, all at $\lambda = 10.6 \mu$ m. The underlying assumption in this plot is that the liquid and solid phase conductivities are the same. The

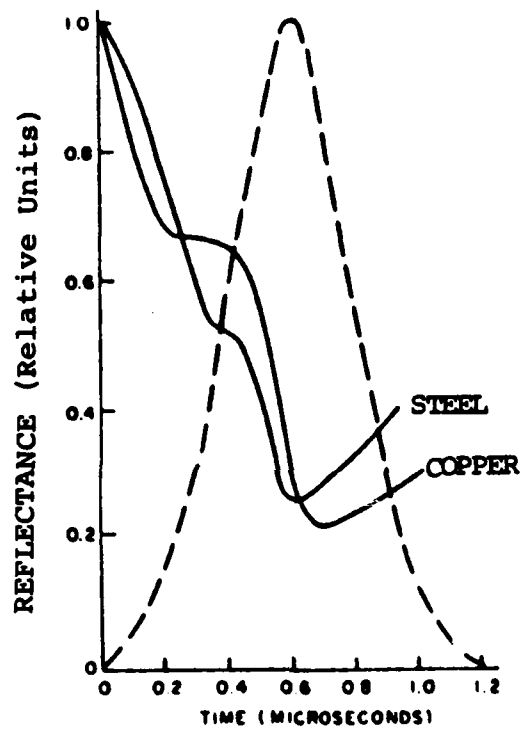


FIGURE 10. REFLECTANCE OF STEEL AND COPPER DURING LASAR IRRADIATION [Ref. 11]

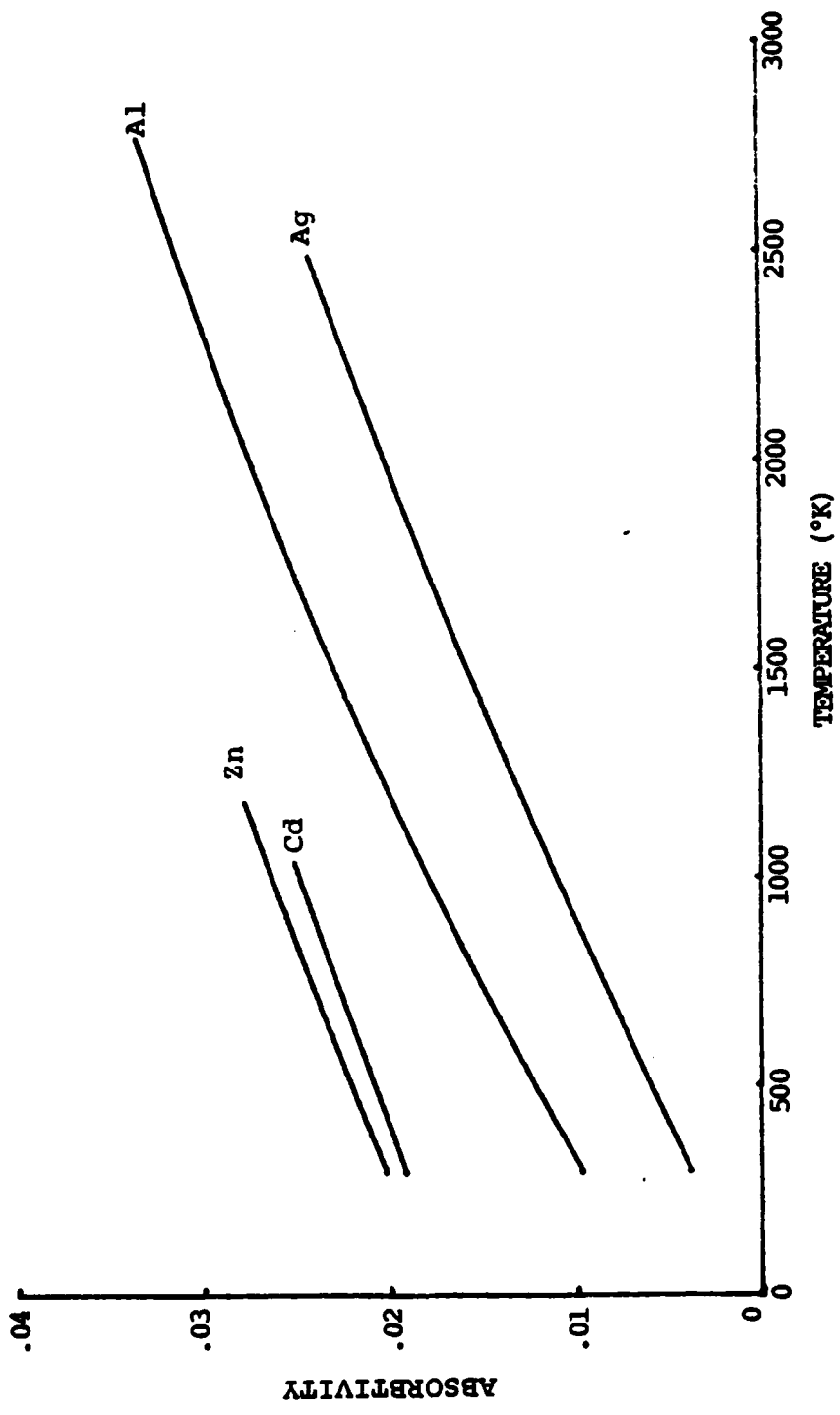


FIGURE 11. ABSORBIVITY VS. TEMPERATURE AT 10.6 μm

plot shows increases in absorbtivity on the order of 1-3 percent.

Thomas and Musal [14] have proposed using an effective value for absorbtivity, A_{eff} , using the following expression:

$$A_{\text{eff}} = (A_v - A_o) \left[\ln(A_v/A_o) - \frac{1}{2}(1 - A_o/A_v) \right]^{-1/2} \quad (\text{eq. 2-2})$$

where A_v is the absorbtivity at vaporization temperature and A_o is at room temperature. Harrach [15] points out that these effective values of absorbtivity may be 5-10 times those at room temperature and cites the Bonch-Bruevich report, [13], as experimental evidence. Again, this could be misleading at low power densities.

Surface preparation plays a large role in the absorbtivity of any practical metal surface and is an empirical matter. Schriempf [16] states some values for Al, Au, Cu, Ag, Ti, Mg and 304-steel. Sandblasting the surface appears to be the best technique resulting in up to ten times the abosrbtivities of ideal surfaces. He does not state the pressure under which his values for absorbtivity were found.

In this paper four materials have been chosen to illustrate various relationships. Aluminum is used because of the vast amount of previous efforts in the laser weapons program. Silver, cadmium and zinc were chosen because of the wide variation in their thermal properties.

III. THERMAL RESPONSES

A. THE MODEL

After the laser energy strikes the target surface, the absorbed energy is converted into thermal energy in the material. The thermal energy so deposited in the surface is distributed in various ways in the material. The immediate result is a sharp rise of the surface temperature. This causes a steep temperature gradient in the material which leads to heat transport from the surface and into the material via heat conduction. Eventually the surface region reaches melting temperature and finally vaporization temperature and the surface melts and vaporizes when enough energy has been absorbed to overcome the heat of melting and vaporization. The exact development of this 3 phase process and the temperature profile into the medium as a function of time is governed by the heat conduction equation together with appropriate boundary conditions.

The heat conduction equation in three dimensions is:

$$\rho_s C_s \frac{\partial T}{\partial t} = \text{div}(K \text{ grad } T) + A \quad (\text{eq. 3-1})$$

where ρ_s is a solid density, C_s is the heat capacity, K is the thermal conductivity and A is the heat produced per unit volume per unit time by the laser source.

$$A = (1 - R) I \frac{4\pi k}{\lambda} e^{-4\pi k z / \lambda} = \frac{\partial F}{\partial z} \quad (\text{eq. 3-2})$$

where $(1 - R)$ is the absorbtivity, I is the laser power density in Watts/cm² and F is the absorbed power density. The term $4\pi k/\lambda$ has the units of cm⁻¹ and is defined as the absorption coefficient where k is the imaginary part of the complex index of refraction. The value $S = \lambda/4\pi k$ is the skin depth. The skin depth is that distance where the intensity of the laser is reduced to $1/e$ of its value at the target surface. In metals, this value is on the order of 10^{-6} cm for wavelenghts in the infrared.

There are different boundary conditions for each phase of the target material. In general even the source term, A , is very complicated as absorbtivity varies with temperature and phase. The laser pulse is directed at the target at an angle and the pulse shape is Gaussian in nature. The target thickness effects the temperature profile in the target material. Even the material constants, C_s , ρ_s , and K change with the wide temperature ranges and phase changes involved between room temperature and vaporization temperature.

In its full generality the problem is quite intractable and for the purpose here, significant simplifications must be made by adopting a number of assumptions and approximations which will now be presented and discussed.

We will begin the discussion by considering the development of the temperature profile for a single solid phase material until vaporization temperature is reached at the surface, that is, we neglect the complication of the liquid phase. Specifically we make these assumptions:

1. It will be assumed that the laser pulse is constant with time and the absorbtivity is also constant, possibly an effective value calculated by the method of Thomas and Musal [14] previously mentioned.

2. The entire problem will be done in one dimension. This one dimensional approach is valid if the laser's beam is perfectly uniform over a large focal area.

3. The materials thermal parameters, ρ_s , C_s , K , etc., are assumed to be temperature independent.

4. Starting temperature for the process will be assumed to be at $T = 0^\circ$ so that all temperatures will be given in $^\circ\text{C}$.

5. The model considered is a laser beam directed at a semi-infinite solid target material, figure 12. Under these conditions an exact solution of the heat conduction equation can be obtained, Carslow and Jaeger [17]. It is also assumed that the laser wavelength is in the infrared region where the skin depth is very small, on the order of 10^{-6} cm.

Under these conditions the heat conduction equation reduces to

$$\frac{\partial^2 T}{\partial z^2} - \frac{1}{\kappa} \frac{\partial T}{\partial t} = \frac{-(1-R)I\alpha e^{-\alpha z}}{K} \quad (\text{eq. 3-3})$$

where $\kappa = K/\rho_s C_s$ and α is the absorption coefficient $4\pi k/\lambda$. The initial and boundary conditions are $T = 0$ at $z = 0$ and

$$-K \frac{\partial T}{\partial z} = (1-R)I = F_0 \quad \text{at} \quad z = 0.$$

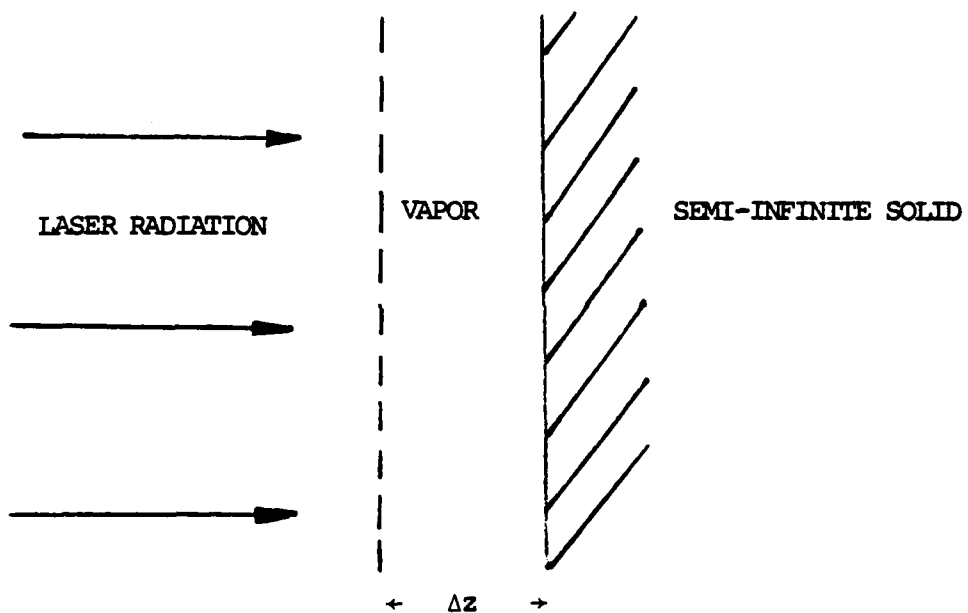


FIGURE 12. MODEL SHOWING LASER RADIATION DIRECTED AT A SEMI-INFINITE SOLID AND THE CREATION OF THE VAPOR FRONT IN DISTANCE Δz

The solution to the problem is:

$$T(z,t) = \frac{2F_0}{K} \left\{ \sqrt{kt/\pi} e^{-z^2/4kt} - \frac{z}{2} \operatorname{erfc} z/2\sqrt{kt} \right\} \quad (\text{eq. 3-4})$$

where

$$\operatorname{erfc} = 1 - \operatorname{erf}$$

and

$$\operatorname{erf} = \frac{2}{\sqrt{\pi}} \int_0^x e^{-x'^2} dx'$$

This model allows us to estimate the time when the surface reaches vaporization temperature.

$$T(0, t_v) \equiv T_v = \frac{2F_0}{K} \sqrt{kt_v/\pi} \quad (\text{eq. 3-5})$$

or

$$t_v = \frac{\pi}{4} \frac{K^2 T_v^2}{\kappa F_0^2} \quad (\text{eq. 3-6})$$

Braginskii, et al., [18], shows experimental support for this equation. Harrach [19] uses the so-called "heat balance integral" method to solve the problem of moving boundaries and obtains a similar result for t_v :

$$t_v = \{3[1 - 2e^{-1}]/\kappa\} \{KT_v/F_0\}^2 \quad (\text{eq. 3-7})$$

The numerical ratio of the two solutions for t_v is 0.99.

The difficulty with this solution to the heat conduction equation is that it does not yet involve phase changes. In order to remove mass from the target surface, first the vaporization temperature must be reached, i.e., enough energy must be deposited into the target surface to raise the temperature from $T_s = 0$ to $T_s = T_v$, or greater ($T_s \equiv$ surface temperature). In addition, enough energy must also be deposited to overcome the latent heats of fusion and vaporization. We now need a simple model for this second stage in the process.

Figure 12 illustrates the model of a semi-infinite solid material. As vaporization is reached, there will be an instantaneous removal of material from the target surface. This results in a moving boundary condition. One would now have to solve a heat conduction problem with these moving boundaries, where the solid interface (again neglecting the liquid phase) moves at a recession velocity U_s .

If this velocity can be calculated, then one could determine the mass removal rate. The solution of this heat conduction problem with its moving boundary in one dimension has been given by Harrach [15] in analytical form using again the "heat balance integral" method. An estimate of this velocity can be obtained from a simple heat balance expression. If Δz is the distance that the interface moves in time Δt then,

$$F_0 \frac{\Delta t}{\Delta z} = L \rho_s + C_s T_v \rho_s \quad (\text{eq. 3-8})$$

where L is the total latent heat from room temperature to vaporization temperature, $L = L_m + L_v$. C_s is some overall heat capacity and ρ_s is an overall density (C_s and ρ_s may be assumed to be those values for the solid to simplify the problem). Then:

$$\frac{\Delta z}{\Delta t} = U_s \quad (\text{eq. 3-9})$$

$$U_s = \frac{F_o}{\rho_s [L + C_s T_v]} \quad (\text{eq. 3-10})$$

This velocity could be thought of as a steady state velocity. This expression for the steady state recession velocity of the evaporating surface is identical to the one Harrach obtains from his model. However, in Harrach's model, at times close to the vaporization time, the surface recession velocity is lower. As no closed form expression exists for times near the vaporization time, he shows a plot obtained numerically to illustrate the buildup of the recession velocity. This solution is reproduced in Figure 13. The result of this analysis is that the value for the steady state surface recession velocity obtained from the general heat balance must be reduced in the region where total laser pulse time is on the order of surface vaporization time.

The considerations discussed above do not take into account yet that the material immediately on the target surface may be at a temperature higher than the vaporization temperature. Anisimov [20] suggests that the surface is indeed at a higher

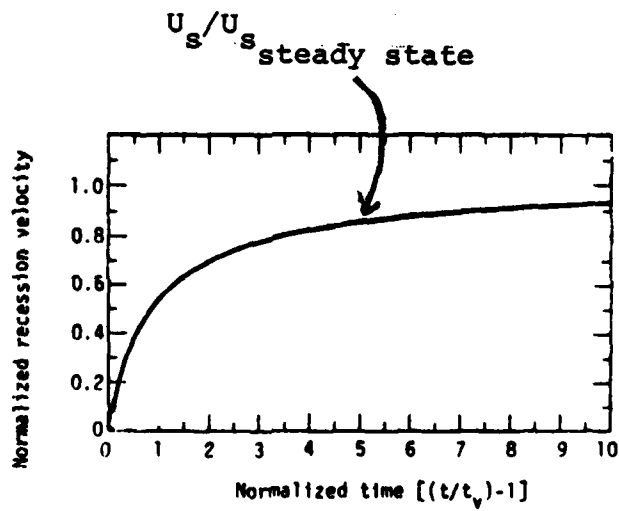


FIGURE 13. NORMALIZED TIME vs. NORMALIZED SURFACE RECESSION VELOCITY. NUMERICAL SOLUTION FROM REF. 16.

temperature caused by an elevated boiling point created by the dynamic and high pressure situation set up at the target surface. We will now expand our simple model somewhat so that it incorporates the idea that the surface may be at a higher temperature than the vaporization temperature and that the vapor, when it does leave the surface, leaves at a velocity of $U_v = \sqrt{k_B T_s / m}$. This would be the z-direction component of the rms thermal velocity where $v_x^2 + v_y^2 + v_z^2 = \langle v \rangle^2$ and k_B is the Boltzman constant. We make the following assumptions for this new model:

B. THE THEORY OF EVAPORATION

1. Assumptions

We will now assume that with the laser energy directed at a target an amount of material of depth Δz is raised above the vaporization temperature and then is removed, Figure 12.

The materials thermal properties, as before, are assumed to be constant with temperature. The liquid and solid phase densities and heat capacities are considered to be approximately equal and the gas phase heat capacity, C_v , is equal to $3/5 C_s$. These assumptions are based on data obtained by experiment, Kelly [21], CRC Handbook [11], and JANAF Thermochemical Tables [22]. In addition, it is assumed that the material in the small increment Δz , to be removed, has heat capacity C_v and solid density, ρ_s , as it has not had time to expand significantly while being heated to a temperature $T_s > T_v$.

2. Temperature Profile in the Material

Under the above conditions and the one dimension model of semi-infinite target thickness, one would expect the temperature profile to be as before (eq. 2-4):

$$T(z,t) = \frac{2F_0}{K} \left\{ \sqrt{\frac{kt}{\pi}} e^{-z^2/4kt} - \frac{z}{2} \operatorname{erfc}[z/2\sqrt{kt}] \right\}$$

This expression is cumbersome to work with as it contains the error function. However, it can be approximated fairly closely. Let D , the diffusion length, be the distance where the temperature decays to $1/e$ of its surface value, T_s . Solving the above equation, the distance D is found to be $D = 0.97\sqrt{kt}$ or simple $D \approx \sqrt{kt}$. It is readily apparent that the temperature profile is of a decaying exponential form. If the diffusion length is used as the spatial decay constant, the equation $T = T_s e^{-z/D}$ can be compared to the actual solution. The comparison, Figure 14, illustrates the close approximation. In fact, the difference is only a few percent and even less if one is interested in a small distance, Δz from the surface, Figure 15.

3. Energy Balance

An energy balance equation can be written to describe the heat conduction problem using the temperature profile

$$T = T_s e^{-z/D};$$

$$F_0 t = \rho_s L \Delta z + \rho_s C_s \int_{\Delta z}^{\infty} T_s e^{-z/D} dz + \rho_s C_s T_v \Delta z + \rho_s C_v \int_0^{\Delta z} (T_s e^{-z/D} - T_v) dz$$

(eq. 3-11)

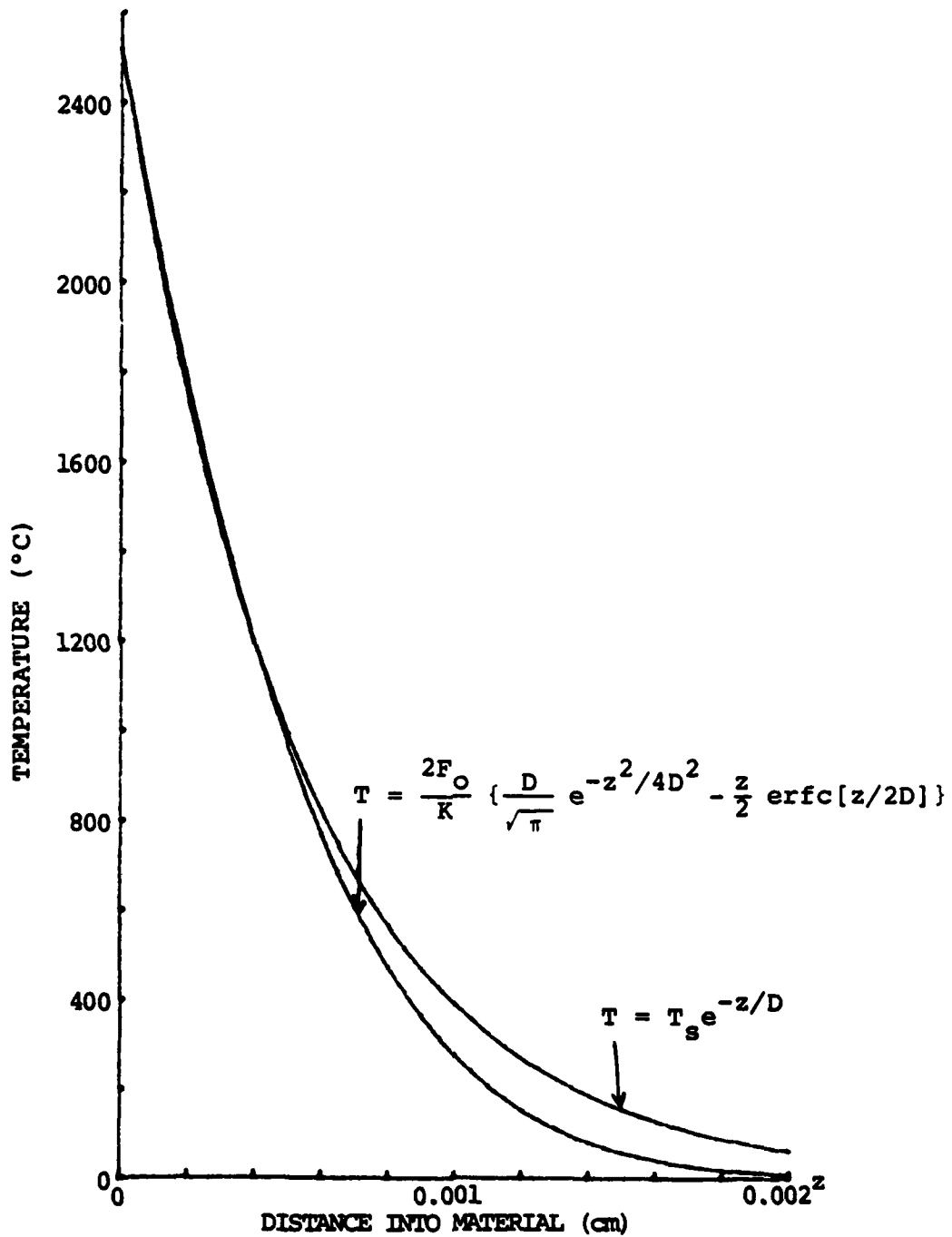


FIGURE 14. COMPARISON OF ACTUAL SOLUTION AND APPROXIMATE SOLUTION FOR $T(z)$ IN THE SEMI-INFINITE SOLID MODEL

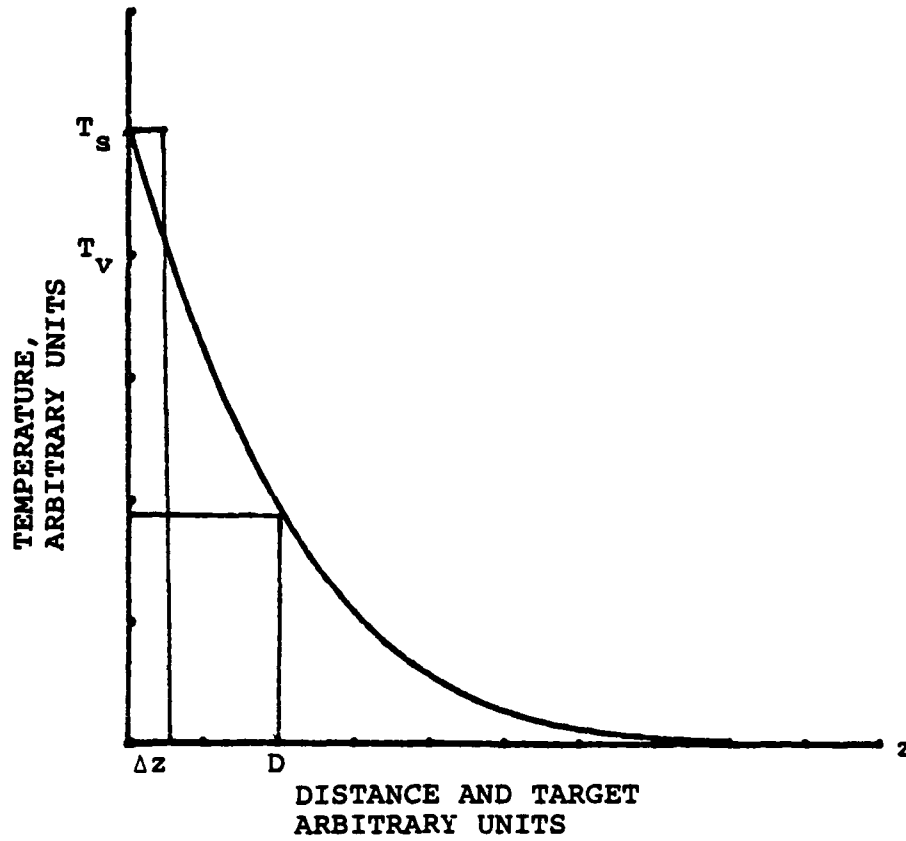


FIGURE 15. TEMPERATURE PROFILE IN A SEMI-INFINITE SOLID SHOWING THE SMALL VAPOR LAYER Δz

In this equation, the terms $\rho_s L \Delta z$ and $\rho_s C_s T_v \Delta z$ are the energy required to raise the small increment Δz to vaporization temperature and overcome the latent heats. The term

$$\rho_s C_s \int_0^{\Delta z} (T_s e^{-z/D} - T_v) dz$$

is the energy required to raise Δz to a temperature $T_s > T_v$. The second term,

$$\rho_s C_s \int_{\Delta z}^{\infty} T_s e^{-z/D} dz$$

is the energy lost due to heat transport into the material. This balance holds in particular for $t = t_p$, the laser pulse length. Using the substitutions

$$T_v = T_s e^{-\Delta z/D} \quad (\text{eq. 3-12})$$

$$D = \sqrt{kt_p} \quad (\text{eq. 3-13})$$

$$\Delta z = D \ln(T_s/T_v) \quad (\text{eq. 3-14})$$

$$C_v = 3/5 C_s \quad (\text{eq. 3-15})$$

the above energy balance equation reduces to:

$$F_0 \sqrt{t_p} = \rho_s \sqrt{k} \left(L \ln(T_s/T_v) + \frac{C_s}{5} [3T_s + 2T_v (1 + \ln T_s/T_v)] \right)$$

(eq. 3-16)

The parameter $F_0 \sqrt{t_p}$ may now be used to calculate the surface temperature from this energy equation. Implicit in this derivation is that the pulse duration, $t = t_p$ is comparatively small while F_0 is large so that the vaporized material has no time to escape during the duration of the pulse and so all the energy arriving must be absorbed in the same material leading to a temperature rise above the vaporization temperature.

Alternatively, keeping $F_0 \sqrt{t_p}$ constant one could produce a laser pulse where $t = t_p$ is very long and F_0 small. In that case the vaporized material escapes from the surface before the pulse terminates. The laser energy heats the next surface layer to the vaporization temperature and as it is reached the surface layer escapes and so on, so that the surface temperature stays essentially at the vaporization temperature. The equation $\Delta z = D \ln(T_s/T_v)$ obviously breaks down in this large t_p case as it predicts $\Delta z = 0$. The equation for $F_0 t_p$ in this situation is

$$F_0 t_p = \rho_s L \Delta z + \rho_s C_s \int_{\Delta z}^{\infty} T_v e^{-z/D} dz + \rho_s C_s T_v \Delta z \quad (\text{eq. 3-17})$$

The expression can now be used to calculate $\Delta z / \sqrt{t_p}$ as a function of $F_0 \sqrt{t_p}$, namely:

$$\frac{\Delta z}{\sqrt{t_p}} = \frac{F_0 \sqrt{t_p} - \rho_s C_s T_v \sqrt{k}}{\rho_s [L + C_s T_v]} \quad (\text{eq. 3-18})$$

4. The Mass Removed

The mass removed during the total time, t_p , can be expressed as $M = \rho_s \Delta z$ where M is the mass expressed in grams per laser focal area. In the case of short pulses we can substitute $\Delta z = D \ln(T_s/T_v)$.

$$M = \rho_s \sqrt{\kappa t_p} \ln(T_s/T_v) \quad (\text{eq. 3-19})$$

we now express M as a function of the parameter $F_o \sqrt{t_p}$.

$$MF_o = F_o \sqrt{t_p} \rho_s \sqrt{\kappa} \ln(T_s/T_v) \quad (\text{eq. 3-20})$$

It must be kept in mind that T_s is also a function of $F_o \sqrt{t_p}$.

In the case of long pulses, when the surface temperature stays close to vaporization temperature we use the expression for $\Delta z/\sqrt{t_p}$ given above.

$$MF_o = \rho_s \Delta z F_o = F_o \sqrt{t_p} \left[\frac{F_o \sqrt{t_p} - \rho_s C_s T_v \sqrt{\kappa}}{(L + C_s T_v)} \right] \quad (\text{eq. 3-21})$$

5. Axial Expansion of the Vapor Jet

For the purpose of the intended application it is of importance to estimate the distance which the vapor front travels during the duration of the laser pulse. If that distance is small, on the order of Δz or less, then no significant expansion has taken place during the energy deposition and we can use the mass removal relation of the high surface temperature

model where $T_s > T_v$. In this case there will be no further experimental constraint. One would fire the main discharge of the high voltage source when the vapor jet has expanded axially across the gap which would be long after the end of the laser pulse.

In the case of long pulses it becomes important how far the vapor surface has traveled when the laser turns off and all mass has been vaporized. That distance traveled must be commensurate with the experimental geometry to give a feasible operating condition.

If t_p is the total pulse time and t_v is the time to vaporization then $(t_p - t_v) = t_f$ is the excess time remaining after vaporization in which the mass located in z can be removed from the target and travel a distance, l , from the target surface. The vaporized particles will travel at a velocity approximately equal to the rms value of velocity in a one dimensional Maxwellian distribution.

$$U_v = \sqrt{k_B T_v / m} \quad (\text{eq. 3-22})$$

Schriempf [16] has obtained the same result for vapor velocity in slightly different form using simple heat balance equations and conservation of mass:

$$U_v = \sqrt{RT/z} \quad (\text{eq. 3-22'})$$

where Z is the atomic weight of the target and R is the gas constant, $R = 8.314 \times 10^7 \text{ erg } ^\circ\text{K mol}^{-1}$. The time to vaporization may be calculated when the expression (eq. 3-18) is applied to the time t_v when the surface reaches vaporization temperature, $T_s = T_v$.

$$t_v = \frac{K^2 T_v^2}{\kappa F_o^2} \quad (\text{eq. 3-23})$$

using again $K = \kappa \rho_s C_s$. This value is fairly consistent with the previously stated values (eq. 3-6) obtained by Carslow and Jaeger [17] and Harrach [15] using completely different methods, and with the experimental results of Braginskii [18]. An expression for the excess time, t_f , can now be written:

$$t_f = t_p - t_v = t_p - \frac{K^2 T_v^2}{\kappa F_o^2} \quad (\text{eq. 3-24})$$

The distance which the vapor surface travels in the axial direction during the pulse time is then

$$l = U_v(t_p - t_v) \quad (\text{eq. 3-25})$$

We will consider a "short" pulse when $l \leq \Delta z$. For the criterion for determining whether we are in the long or short pulse region, we can safely use the expression for the long pulse which does not involve the elevated surface temperature.

$$\Delta z = \sqrt{t_p} \left[\frac{F_o \sqrt{t_p} - \rho_s C_s T_v \sqrt{k}}{\rho_s (L + C_s T_v)} \right] \quad (\text{Eq. 3-26})$$

Combining the above expression for l and Δz we have a condition for short pulse:

$$U_v \left(t_p - \frac{K^2 T_v^2}{\kappa F_o^2} \right) \leq \sqrt{t_p} \left[\frac{F_o \sqrt{t_p} - \rho_s C_s T_v \sqrt{k}}{\rho_s (L + C_s T_v)} \right] \quad (\text{eq. 3-27})$$

which can be rewritten to give the condition,

$$F_o \geq \frac{U_v \left[(F_o \sqrt{t_p})^2 - \frac{K^2 T_v^2}{\kappa} \right]}{F_o \sqrt{t_p} \left[\frac{F_o \sqrt{t_p} - \rho_s C_s T_v \sqrt{k}}{\rho_s (L + C_s T_v)} \right]} \quad (\text{eq. 3-28})$$

If this condition is not satisfied we must calculate the value of l where

$$l = U_v (t_p - t_v) = U_v \left(t_p - \frac{K^2 T_v^2}{\kappa F_o^2} \right) \quad (\text{eq. 3-29})$$

or

$$l = \frac{U_v}{F_o^2} \left[(F_o \sqrt{t_p})^2 - \frac{K^2 T_v^2}{\kappa} \right] \quad (\text{eq. 3-30})$$

6. Density and Pressure in the Plume

Once expressions are found for Δz in the two cases, long and short pulse, then we can calculate the density and pressure of the vapor plume of the surface. Conservation of

mass tells us that

$$\rho_v U_v = \rho_s U_s \quad (\text{eq. 3-31})$$

where ρ_v is the vapor density as Δz expands into the cavity. In the case of short pulses $\Delta z = D \ln(T_s/T_v)$, where $D = \sqrt{\kappa t_p}$, $U_s = \Delta z / (t_p - t_v)$ and $U_v = \sqrt{k_b T_s / m}$. Substituting, one can find the expression for ρ_v .

$$\rho_v = \frac{\rho_s \sqrt{\kappa t_p} \ln(T_s/T_v)}{U_v (t_p - t_v)} \quad (\text{eq. 3-32})$$

$$t_v = \frac{K^2 T_v^2}{\kappa F_o^2}$$

$$\frac{\rho_v}{F_o} = \frac{\rho_s F_o \sqrt{t_p} [\sqrt{\kappa} \ln(T_s/T_v)]}{U_v [(F_o \sqrt{t_p})^2 - \frac{K^2 T_v^2}{\kappa}]} \quad (\text{eq. 3-33})$$

As before, ρ_v / F_o is expressed as a function of $F_o \sqrt{t_p}$.

The pressure, P , is estimated from the dynamic pressure,

$$P = \rho_v U_v^2,$$

$$\frac{P}{F_o} = \frac{\rho_v U_v^2}{F_o}$$

$$\frac{P}{F_o} = \rho_s U_v \frac{[F_o \sqrt{t_p} - \sqrt{\kappa} \ln T_s/T_v]}{[(F_o \sqrt{t_p})^2 - \frac{K^2 T_v^2}{\kappa}]} \quad (\text{eq. 3-34})$$

In the case of long pulses, the expression for ρ_v/F_0 is different. As before,

$$\frac{\Delta z}{\sqrt{t_p}} = \frac{F_0 \sqrt{t_p} - \rho_s C_s T_v \sqrt{\kappa}}{\rho_s [L + C_s T_v]} \quad (\text{eq. 3-35})$$

Here, one can use

$$U_s = \frac{\Delta z}{(t_p - t_v)} = \frac{\Delta z}{\sqrt{t_p}} \frac{1}{(\sqrt{t_p} - \frac{t_v}{\sqrt{t_p}})} \quad (\text{eq. 3-36})$$

Again using conservation of mass, $\rho_v U_v = \rho_s U_s$ one can substitute and arrive at the equation for ρ_v/F_0 :

$$\frac{\rho_v}{F_0} = \frac{[F_0 \sqrt{t_p} - \rho_s C_s T_v \sqrt{\kappa}]}{U_v [L + C_s T_v] [F_0 \sqrt{t_p} - \frac{\kappa^2 T_v^2}{\kappa F_0 \sqrt{t_p}}]} \quad (\text{eq. 3-37})$$

The pressure is found in the same manner as for the short pulse and is:

$$\frac{P}{F_0} = U_v \frac{[F_0 \sqrt{t_p} - \rho_s C_s T_v \sqrt{\kappa}]}{[L + C_s T_v] [F_0 \sqrt{t_p} - \frac{\kappa^2 T_v^2}{\kappa F_0 \sqrt{t_p}}]} \quad (\text{eq. 3-38})$$

7. Limit on T_s to Avoid Ionization

The question now is what value can T_s take in the elevated surface temperature model. As pointed out previously, if the temperature is allowed to become on the order of 2-3 eV,

then the ionization degree reaches a critical value where the vapor plume begins absorbing the laser's radiation. This absorption by the plume occurs at plasma densities given by the plasma frequency

$$\omega_p = n_e e^2 / \epsilon_0 m_0 \quad (\text{eq. 3-39})$$

where m_0 is the free electron density in the plume. If electron densities are allowed to rise above this cut-off value for propagation of electromagnetic waves, then strong absorption will occur in the low-temperature plasma plume. This condition for cut-off can be rewritten as

$$n_e > 1.12 \times 10^{13} / \lambda_p^2 \quad (\text{eq. 3-40})$$

where λ_p is now the laser wavelength in centimeters and n_e is the electron density in electrons per cubic centimeters. If we assume one free electron per atom and solid density in the vapor at the target surface then Saha's equation, [23], can be used to predict the maximum allowable surface temperature to avoid cut-off degrees of ionization

$$\frac{n_e}{n_n} = 2.4 \times 10^{15} T_s^{3/2} e^{-11600U_i/T_s} \quad (\text{eq. 3-41})$$

where

$$n_n \equiv \text{neutral particle density}$$

U_i \equiv ionization potential of the target material
in eV.

The degree of ionization is given by n_e/n_t where $n_t = n_e + n_n$
and can be written as follows:

$$2.4 \times 10^{-15} T_s^{3/2} e^{-11600U_i/T_s} \equiv C,$$

and

$$\frac{n_e}{n_t} = \frac{-C + \sqrt{C^2 + 4n_t C}}{2n_t} \quad (\text{eq. 3-42})$$

We now have a rough temperature criterion for significant
plasma production to occur. Namely, arrange for the value
 $F_0 \sqrt{t_p}$ such that T_s will always be below the value required
for cut-off.

$$n_e \leq 1.12 \times 10^{13} / \lambda_p^2$$

IV. RADIAL EXPANSION OF THE VAPOR PLUME

As the vapor plume propagates along the axis it will also expand radially. To assess the feasibility of the approach one needs to know whether the radial expansion is commensurate with the expected geometry. Therefore we need an estimate of the radial expansion as a function of the distance from the target surface.

A simple estimate can be obtained if we assume that the speed with which the plume radius expands is equal to the sound speed, see Figure 16.

We consider therefore a slice of the plume which has traveled along the axis for a time, t . For the purpose of this discussion we neglect any expansion of the slice in the axial direction due to possible pressure gradients in that direction. As the slice propagates along the axis and expands radially the temperature and density must change and so the sound speed is a function of the temperature which is a function of the z -position on the axis.

$$\frac{dR(t)}{dt} = a(T) = \sqrt{C_p(\gamma-1)T} \quad (\text{eq. 4-1})$$

The expansion is assumed to be adiabatic so that

$$\frac{P_1}{P_0} = \left(\frac{\rho_1}{\rho_0}\right)^\gamma = \left(\frac{T_1}{T_0}\right)^{\frac{\gamma}{\gamma-1}} \quad (\text{eq. 4-2})$$

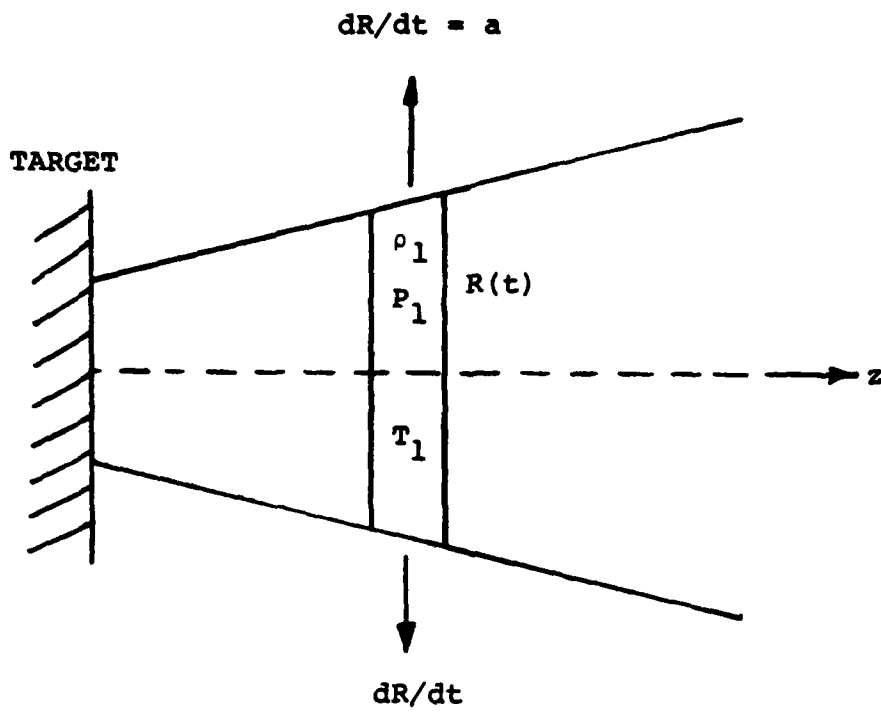


FIGURE 16. MODEL ILLUSTRATING THE RADIAL EXPANSION OF THE VAPOR

where T_0 , P_0 and ρ_0 are measured at the target surface and T_1 , P_1 , and ρ_1 , are taken to be at some later time, after the vapor has expanded. The quantity γ is the ratio of specific heats and is 1.66 for monatomic metal vapor.

For small changes in density and temperature, $d\rho$ and dT ,

$$\left(\frac{\rho + d\rho}{\rho}\right)^\gamma = \left(\frac{T + dT}{T}\right)^{\gamma/\gamma-1} \quad (\text{eq. 4-3})$$

or,

$$\frac{\rho + d\rho}{\rho} = \left(\frac{T + dT}{T}\right)^{1/\gamma-1} \quad (\text{eq. 4-4})$$

Using binomial expansion for the temperature term yields

$$1 + \frac{d\rho}{\rho} = 1 + \left(\frac{1}{\gamma-1}\right) \frac{dT}{T} \quad (\text{eq. 4-5})$$

or simply,

$$\frac{d\rho}{\rho} = \left(\frac{1}{\gamma-1}\right) \frac{dT}{T} \quad (\text{eq. 4-6})$$

Since the density decreases with increasing radius (again assuming that the thickness of each slice does not change) one can write

$$(\rho + d\rho)(R + dR)^2 = \rho R^2, \quad (\text{eq. 4-7})$$

and

$$\left(1 + \frac{d\rho}{\rho}\right) \left(1 + \frac{dR}{R}\right)^2 = 1 \quad (\text{eq. 4-8})$$

Again using binomial expansion for the quadratic in R and substituting for $d\rho/\rho$ the above expression yields

$$\left(1 + \frac{1}{\gamma-1} \frac{dT}{T}\right) \left(1 + \frac{2dR}{R}\right) = 1 \quad (\text{eq. 4-9})$$

By assuming the second order $(dT)(dR)$ term to be negligible compared to the other terms and rewriting gives,

$$\frac{2dR}{R} = - \frac{1}{\gamma-1} \frac{dT}{T} \quad (\text{eq. 4-10})$$

R_0 is now taken to be the initial plume radius which is the laser's focal radius. T_0 is assumed to be the surface temperature. Integrating both sides yields

$$\left(\frac{R}{R_0}\right)^{-2} = \left(\frac{T}{T_0}\right)^{1/\gamma-1} \quad (\text{eq. 4-11})$$

or,

$$\left(\frac{R}{R_0}\right)^{1-\gamma} = \left(\frac{T}{T_0}\right)^{1/2} \quad (\text{eq. 4-12})$$

Substituting $\sqrt{T} = a/\sqrt{C_p(\gamma-1)}$ and $a = dR/dt$ yields

$$\left(\frac{R}{R_0}\right)^{1-\gamma} = \frac{dR/dt}{\sqrt{C_p(\gamma-1)T_0}} \quad (\text{eq. 4-13})$$

The term $\sqrt{C_p(\gamma-1)T_0}$ is simply U_v , the initial vapor velocity.
Therefore,

$$\left(\frac{R}{R_0}\right)^{1-\gamma} = \frac{1}{U_v} \frac{dR}{dt} \quad (\text{eq. 4-14})$$

and,

$$\frac{dR}{R^{1-\gamma}} = \frac{U_v}{R_0^{1-\gamma}} dt \quad (\text{eq. 4-15})$$

Integrating both sides:

$$\int_{R_0}^R \frac{dR}{R^{1-\gamma}} = \frac{U_v}{R_0^{1-\gamma}} \int_{t_v}^t dt \quad (\text{eq. 4-16})$$

or,

$$\left(\frac{R}{R_0}\right)^\gamma = 1 + \frac{\gamma U_v}{R_0}(t - t_v) \quad (\text{eq. 4-17})$$

But, $U_v = (t - t_v)$ is the axial distance, l , that the vapor plume will travel in the cavity. Therefore,

$$\left(\frac{R}{R_0}\right)^\gamma = 1 + \frac{\gamma l}{R_0} \quad (\text{eq. 4-18})$$

or,

$$R = R_0 [1 + \gamma l / R_0]^{1/\gamma} \quad (\text{eq. 4-19})$$

This expression can now be used to calculate the radial expansion as a function of the axial distance traveled z . The previously derived equation for temperature can be used to calculate T at that distance R :

$$\left(\frac{R}{R_0}\right)^{-2} = \left(\frac{T}{T_0}\right)^{1/\gamma-1} \quad (\text{eq. 4-20})$$

The density and pressure can be obtained using the adiabatic expansion relationship:

$$\begin{aligned} \left(\frac{R_0}{R}\right)^2 &= \left(\frac{P}{P_0}\right)^{1/\gamma} \\ &= \left(\frac{\rho}{\rho_0}\right) = \left(\frac{T}{T_0}\right)^{1/\gamma-1} \end{aligned} \quad (\text{eq. 4-21})$$

It must be noted again that this calculation gives merely an estimate for z and in a more rigorous model would have to be replaced by a proper fluid dynamical model.

V. RESULTS

There are now two cases of the mass removal process. Both involve F_0 low enough to avoid significant ionization so that all the laser's energy is either absorbed at the material's surface or is reflected. There will be little absorption in the vapor plume.

A. CASE I. SMALL PULSE TIME

This is the situation where the following condition is met:

$$F_0 > \frac{U_v \left[(F_0 \sqrt{t_p})^2 - \frac{K^2 T_v^2}{\kappa} \right]}{F_0 \sqrt{t_p} \left[\frac{F_0 \sqrt{t_p} - \rho_s C_s T_v \sqrt{\kappa}}{\rho_s (L + C_s T_v)} \right]}$$

In this case the surface temperature will be elevated slightly above the vaporization temperature and is described by equation (3-28). Figure 17 is a plot of the elevated surface temperature, T_s as a function of $F_0 \sqrt{t_p}$, the controlling parameter at 10 μm . On this plot, the lowest value of T_s for each material corresponds to T_v and $F_0 \sqrt{t_p}$. The maximum value for T_s is the temperature at which there will be cut-off and significant absorption of the radiation occurs by the vapor plume due to ionization. That maximum T_s was calculated by first finding the maximum allowed free electron density, n_e , given by equation (3-40). Next, calculate the maximum allowed degree of ionization, n_e/n_t . Then, use Saha's

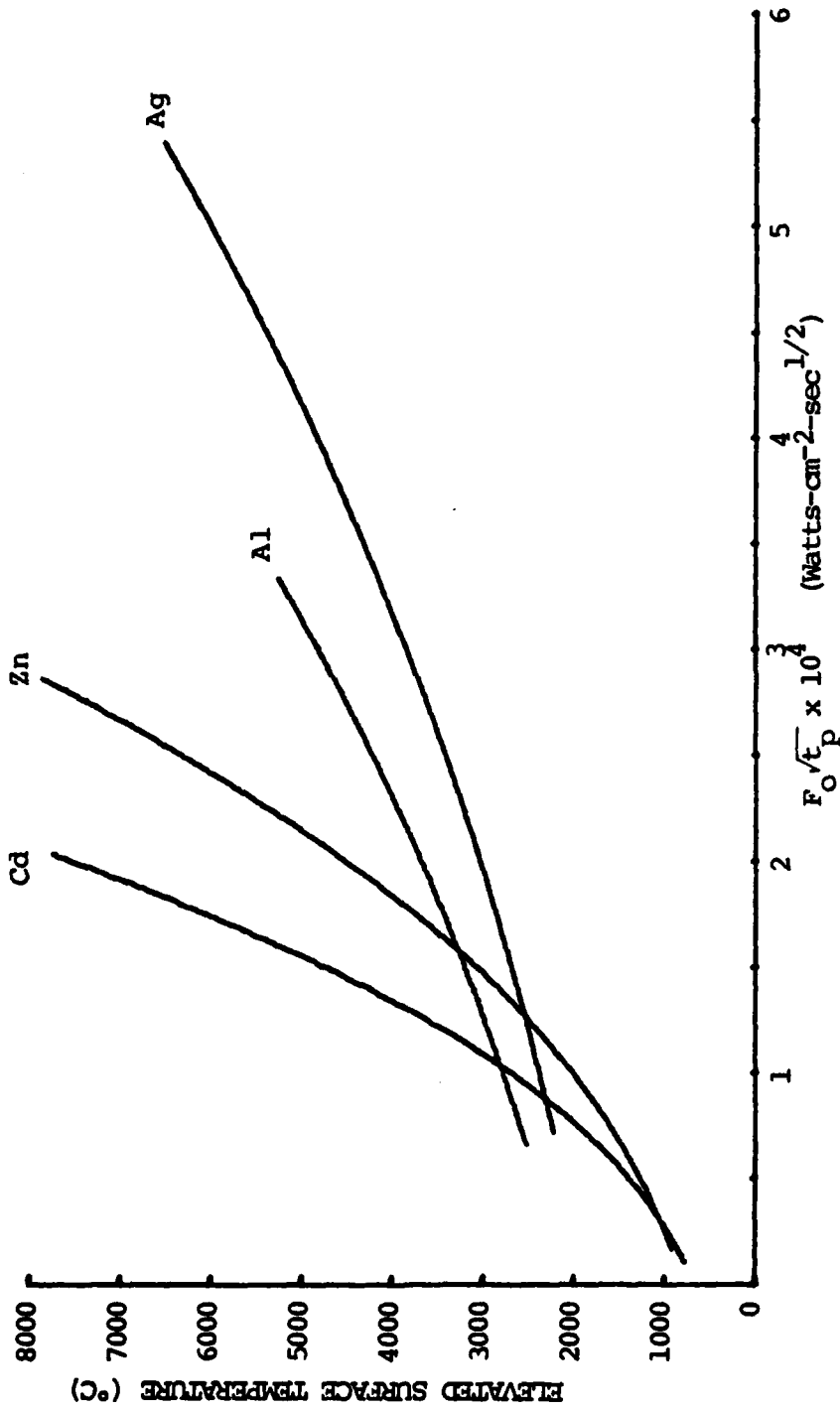


FIGURE 17. ELEVATED SURFACE TEMPERATURE vs. $F_o \sqrt{t_p}$ FOR CASE I

equation, equation (2-42) to find the maximum allowed T_s . It will be a different value for each material and wavelength, and can vary by several thousands of degrees.

Figure 18 is a plot of MF_0 vs. $F_0\sqrt{t_p}$ for Case I of short laser pulses and Case II of long time pulses from equations 3-20 and 3-21. The difference between Case I and Case II is slight except at high values of $F_0\sqrt{t_p}$. Case I gives a lower value of MF_0 than Case II. In this plot, the maximum value for Case I corresponds to a $F_0\sqrt{t_p}$ and a T_s where plume absorption begins. Case II was also plotted to that same value of $F_0\sqrt{t_p}$, however, the surface temperature does not rise above vaporization temperature and could be plotted to much higher values of $F_0\sqrt{t_p}$.

B. CASE II. LONG PULSE TIMES

Case II is the situation where the condition on

$$F_0 > \frac{U_v [(F_0\sqrt{t_p})^2 - \frac{K^2 T_v^2}{\kappa}]}{F_0\sqrt{t_p} \left[\frac{F_0\sqrt{t_p} - \rho_s C_s T_v \sqrt{\kappa}}{\rho_s (L + C_s T_v)} \right]}$$

is not met. This is the case of low F_0 and long t_p . The surface temperature remains at essentially T_v . In this case absorption by the plume never occurs.

C. MASS REMOVAL CALCULATION

A numerical example is now presented to show the use of the various equations and to illustrate that masses on the

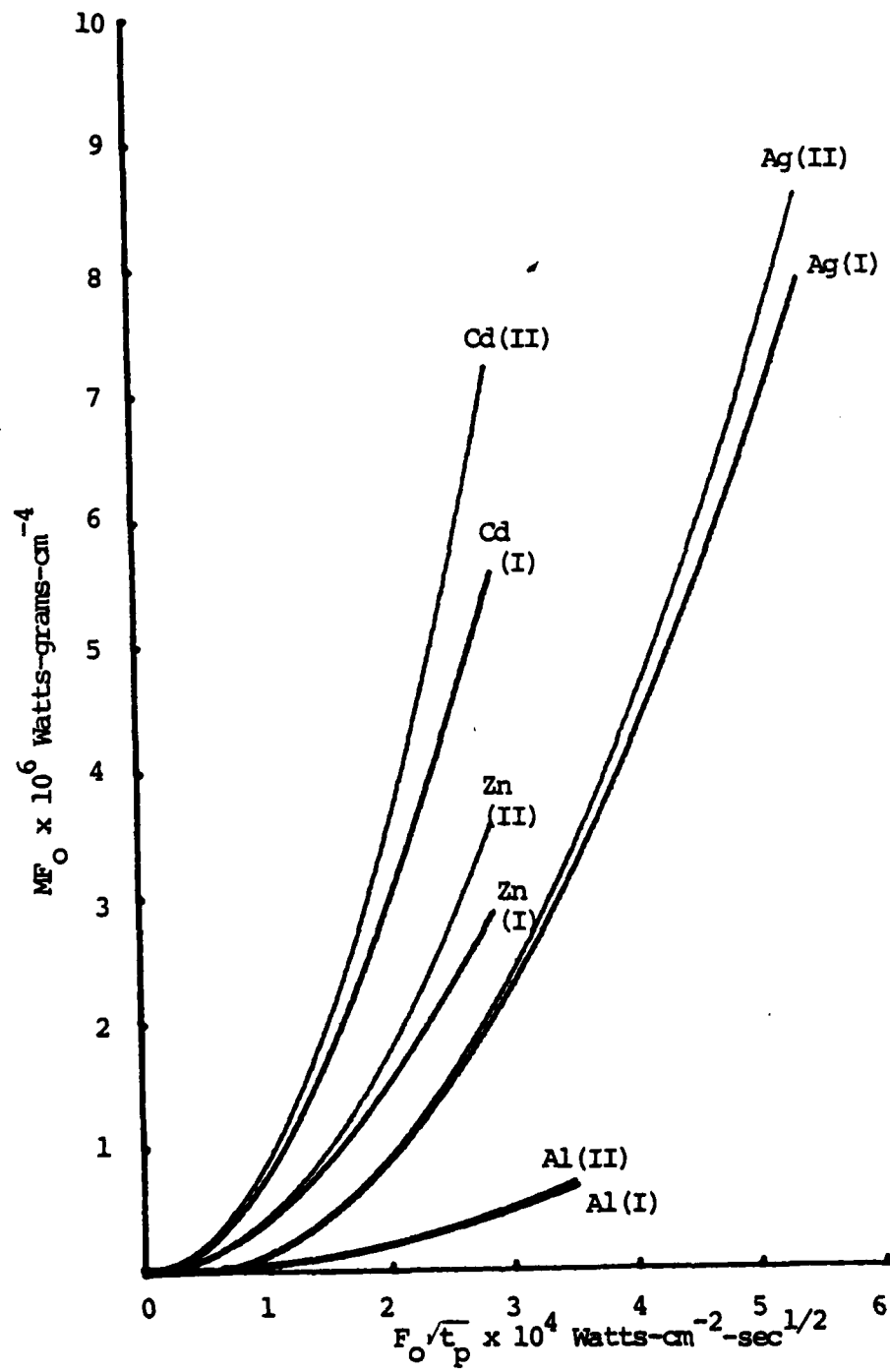


FIGURE 18. MF_0 vs. $F_0 \sqrt{t_p}$ FOR CASE I, SHORT PULSE AND CASE II, LONG PULSE

order of milligrams could, theoretically, be removed without plasma production at a materials surface. The material chosen for the example is Zn, as it has a relatively high Z-number and low latent heats and vaporization temperature. The following thermal properties are from Table II:

$$\rho_s = 7.13 \text{ g/cm}^3$$

$$C_s = 0.39 \text{ Joules/g}^\circ\text{K}$$

$$\kappa = 0.41 \text{ cm}^2/\text{sec}$$

$$K = 1.13 \text{ Watts/cm } ^\circ\text{K}$$

$$T_v = 907 \text{ }^\circ\text{C}$$

$$Z = 65.38$$

Let us assume that $F_o \sqrt{t_p} = 10^4 \text{ Watts sec}^{1/2}/\text{cm}^2$ and that the laser's focal area = 10^{-1} cm^2 . First the condition for the two cases must be tested from equation 3-28, Figure 19.

$$F_o = 6.22 \times 10^8 \text{ Watts/cm}^2$$

TABLE II
THERMAL PROPERTIES OF SELECTED MATERIALS

Material	Diffusivity ($\text{cm}^{2/5}$)	Thermal Conductivity ($\text{W/cm} \cdot ^\circ\text{K}$)	Specific Heat ($\text{J/g}^\circ\text{K}$)	Density (g/cm^3)	Heat of Melting (J/g)	Heat of Vaporization (J/g)	Vaporization Temperature ($^\circ\text{C}$)	Vaporization Ionization Potential (ev)
Al	0.85 [16]	2.40 [16]	1.05 [16]	2.70 [16]	395.6 [24]	10875 [1]	2520 [16]	5.98 [24]
Ag	1.63 *	4.10 [11]	0.24 [24]	10.50 [24]	104.7 [24]	2355 [3]	2212 [24]	7.57 [24]
Cd	0.46 *	0.92 [11]	0.23 [24]	8.65 [24]	54.0 [24]	890 [3]	765 [24]	8.99 [24]
Zn	0.41 *	1.13 [11]	0.39 [24]	7.13 [24]	102.1 [24]	1754 [3] ³	907 [24]	9.39 [24]

* Diffusivity was calculated using $\kappa = K/\rho C$

If F_0 is chosen to be less than 6.22×10^8 then Case II must be used. If not, Case I must be used. Let us choose $F_0 = 2 \times 10^6$ Watts/cm². Then,

$$\begin{aligned}t_p &= (10^4/F_0)^2 = 2.5 \times 10^{-5} \\ &= 25 \text{ } \mu\text{sec.}\end{aligned}$$

From equation 3-21 or Figure 18 for Case II,

$$MF_0 = 3.79 \times 10^4 \text{ Watts grams cm}^{-4}$$

or,

$$M = 3.79 \times 10^{-2} \text{ grams cm}^{-2}.$$

If the focal area is assumed to be 10^{-1} cm², then the mass removed is 3.79 mg. The axial expansion during the pulse t_p is:

$$l = U_s(t_p - t_v) = 0.83 \text{ cm.}$$

The density and pressure before radial expansion can be found using equations 3-37 and 3-38.

$$\rho_v = 2.29 \times 10^{-2} \text{ g/cm}^3$$

$$P_v = 2.65 \times 10^7 \text{ ergs/cm}^2 = 3.85 \text{ psi.}$$

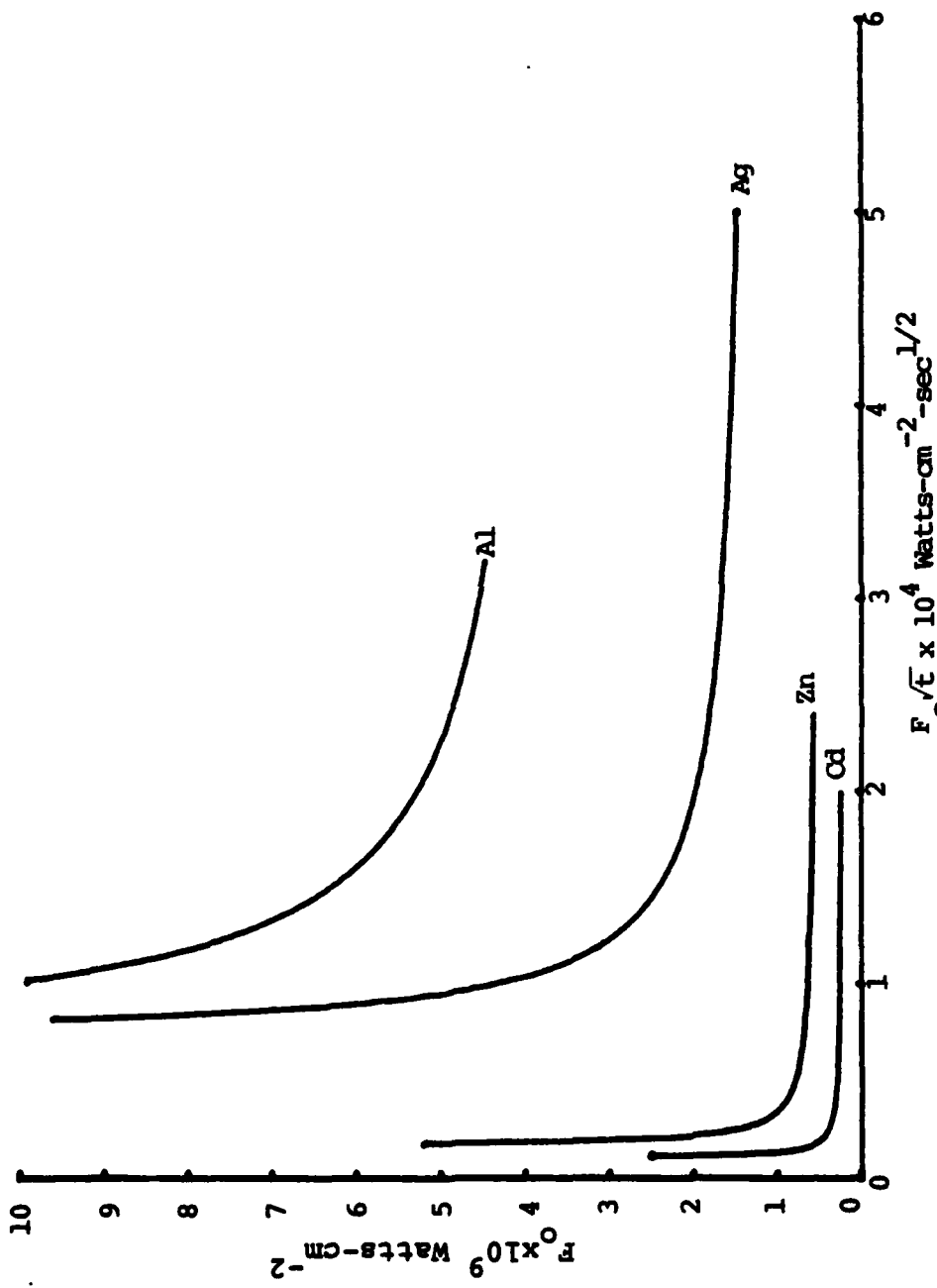


FIGURE 19. CONDITION FOR CASE I OR CASE II, EQUATION 2-28

If the anode-cathode separation is assumed to be 4 cm and $R_0 = 0.18$ cm, then the radial expansion at $z = 4$ cm can be found from equation 4-19.

$$R = 1.65 \text{ cm.}$$

The pressure, density and temperature after radial expansion to $R = 1.65$ cm and axial expansion to $z = 4$ cm are calculated from equation 4-21.

$$P = 2.39 \times 10^{-3} \text{ psi}$$

$$\rho = 2.73 \times 10^{-4} \text{ g/cm}^3$$

$$T = 61.5 \text{ }^\circ\text{K}$$

This shows that a relatively low power CO_2 laser pulse of 2×10^6 Watts/cm² of 25 μ sec duration can produce a zinc vapor plume with the desired mass and dimensions.

VI. CONCLUSION

As stated in the Introduction, the purpose of this study was to assess the general feasibility of using a laser's radiation to remove masses on the order of milligrams from a target's surface. This material will fill a discharge channel between the anode and cathode of a high voltage pulse device which, when activated, will couple electrical energy into the material in the discharge channel causing the atoms to undergo electronic transitions and then giving off intense x-rays.

The model presented herein is a heat balance model at the target surface. No attempt has been made to solve the complicated heat conduction equations with its associated moving boundaries. In this model, the controlling parameter is $F_0 \sqrt{t}$, the absorbed power density and the laser pulse time. Two separate cases emerge from the model. Case I is the case where, keeping $F_0 \sqrt{t}$ constant, F_0 takes on a relatively high value while the pulse time is small. Case II considers the situation of the same value for $F_0 \sqrt{t}$ but smaller F_0 and longer pulse time. Using this model, theoretically, masses of the order of milligrams can be removed from metallic surfaces with relatively low power densities.

The mass removal model also predicts low temperatures at the target surface and thus in the discharge channel. As stated in section II this will produce low degrees of

ionization. In order to increase the coupling efficiency of the electrical energy into the vapor plume, the ionization level must be increased. This could be done by increasing the laser power level towards the end of the pulse or by using microwave radiation after the plume has propagated into the discharge channel and prior to the application of the high voltage pulse.

In addition to mass removal, the controlling parameter $F_0 \sqrt{t_p}$ is used to predict the temperature, density and pressure of the vapor plume as it begins to propagate. As the plume propagates into the vacuum chamber it undergoes axial and radial expansion. Temperature, density and pressure decrease during this process and can be predicted using a model of adiabatic jet expansion presented in section II.

The mass removal model predicts that a laser can remove masses from a target surface large enough to be used in the proposed experiment. In addition, the expansion of the vapor plume is sufficiently small as not to damage the components located in the vacuum chamber. Using a long laser pulse (Case II) the proposed technique shows that the vapor in the discharge channel is relatively cold and requires pre-ionization prior to application of the high voltage pulse.

APPENDIX A

The interactions of materials with electromagnetic waves is formulated on the basis of Maxwell's equation:

$$\nabla \times \bar{E} = -\mu_0 \frac{\partial \bar{H}}{\partial t} - \mu_0 \frac{\partial \bar{M}}{\partial t}$$

$$\nabla \times \bar{H} = \epsilon_0 \frac{\partial \bar{E}}{\partial t} + \frac{\partial \bar{P}}{\partial t} + \bar{J}$$

$$\nabla \cdot \bar{E} = -\frac{1}{\epsilon_0} \nabla \cdot \bar{P} + \rho_e$$

$$\nabla \cdot \bar{H} = -\nabla \cdot \bar{M}$$

where,

\bar{E} \equiv Electric field

\bar{H} \equiv Magnetic field

\bar{M} \equiv Magnetization

\bar{J} \equiv Current density

\bar{P} \equiv Polarization

ϵ_0 \equiv Dielectric constant

μ_0 \equiv Magnetic permeability

ρ_e \equiv Charge density

We will assume that our concern is with non-magnetic, electrically neutral materials. In conducting mediums it is the contribution from the free electrons that predominate. This will allow us to ignore the polarization effects. Maxwell's equations now reduce to the following:

$$\nabla \times \bar{E} = -\mu_0 \frac{\partial \bar{H}}{\partial t}$$

$$\nabla \times \bar{H} = \epsilon_0 \frac{\partial \bar{E}}{\partial t} + \bar{J}$$

$$\nabla \cdot \bar{E} = 0$$

$$\nabla \cdot \bar{H} = 0$$

The general wave equation for \bar{E} is then found by taking the curl of the first equation and the time derivative of the second equation.

$$\nabla \times \nabla \times \bar{E} = \nabla \times \left(-\mu_0 \frac{\partial \bar{H}}{\partial t} \right)$$

$$\frac{\partial}{\partial t} (\nabla \times \bar{H}) = \frac{\partial}{\partial t} \left(\epsilon_0 \frac{\partial \bar{E}}{\partial t} \right) + \frac{\partial \bar{J}}{\partial t}$$

Using the vector identity

$$\nabla \times \nabla \times \bar{E} = \nabla (\nabla \cdot \bar{E}) - \nabla^2 \bar{E}$$

and noting that $\nabla \cdot \bar{E} = 0$, we can exchange the order of differentiation in the electric field equation and multiply the magnetic field equation by μ_0 to give

$$\nabla^2 \bar{E} = \mu_0 \frac{\partial}{\partial t} (\nabla \times \bar{H})$$

$$0 = -\mu_0 \frac{\partial}{\partial t} (\nabla \times \bar{H}) + \mu_0 \epsilon_0 \frac{\partial^2 \bar{E}}{\partial t^2} + \mu_0 \frac{\partial \bar{J}}{\partial t}$$

Adding and substituting $c^2 = \frac{1}{\mu_0 \epsilon_0}$,

$$\nabla^2 \bar{E} - \frac{1}{c^2} \frac{\partial^2 \bar{E}}{\partial t^2} = \mu_0 \frac{\partial \bar{J}}{\partial t}$$

Plane harmonic waves solutions for the electric field are of the form

$$\bar{E} = E_0 \exp\{[-2\pi kz/\lambda] + [i\omega(t - nz/C)]\}$$

where

$n \equiv$ Real part of index of refraction

$k \equiv$ imaginary part of index of refraction.

Substituting this into the electric field equation derived above along with Ohm's law, $\bar{J} = \sigma \bar{E} = -Nev$, gives us an expression for $n-ik$.

$$n - ik = \sqrt{1 - i\sigma/\epsilon_0 \omega}$$

σ is the conductance and is in general a complex quantity, namely $\sigma = \sigma_1 - i\sigma_2$. Then,

$$n - ik = \sqrt{1 - \frac{\sigma_2}{\epsilon_0 \omega} - \frac{i\sigma_1}{\epsilon_0 \omega}}$$

In order to evaluate n and k one can use the Drude-Lorentz model. In this model the atom and its outermost electron are assumed to follow the equation governing the motion of the harmonic oscillator:

$$m^* \frac{d\bar{v}}{dt} + \frac{m^* \bar{v}}{\tau} = -e \bar{E}$$

where

m^* \equiv effective mass

τ \equiv relaxation time.

If a solution of the form $e^{-i\omega t}$ is assumed for \bar{v} and \bar{E} , and Ohm's law, $\sigma \bar{E} = -Ne\bar{v}$ is substituted for \bar{v} , one can show that

$$\sigma = \frac{Ne^2 \tau}{m^* (1 + \omega^2 \tau^2)}$$

By separation of the real and imaginary parts one can write an expression for σ_1 and σ_2 .

$$\sigma_1 = \frac{\sigma_0}{1 + \omega^2 \tau^2}$$

$$\sigma_2 = \frac{\sigma_0 \omega \tau}{1 + \omega^2 \tau^2}$$

where σ_0 is the static of dc conductivity. As the frequency approaches zero, $\omega \rightarrow 0$,

$$\sigma_0 = \frac{Ne^2 \tau}{m^*}$$

The real and imaginary parts of the index of refraction, n and k can now be found using a complex identity:

$$2n^2 = \left(1 - \frac{\sigma_2}{\epsilon_0 \omega}\right) + \sqrt{\left(1 - \frac{\sigma_2}{\epsilon_0 \omega}\right)^2 + \frac{\sigma_1}{\epsilon_0 \omega}}$$

$$2k^2 = -\left(1 - \frac{\sigma_2}{\epsilon_0 \omega}\right) + \sqrt{\left(1 - \frac{\sigma_2}{\epsilon_0 \omega}\right)^2 + \frac{\sigma_1}{\epsilon_0 \omega}}$$

τ can now be eliminated from the expression for σ_1 , and σ_2 by using the equation for σ_0 . The resulting equations for σ_1 and σ_2 are:

$$\sigma_1 = \frac{\sigma_0}{1 + \omega^2 \left(\frac{m^* \sigma_0}{Ne^2}\right)^2}$$

$$\sigma_2 = \frac{\sigma_0^2 \frac{m^* \sigma_0}{Ne^2}}{1 + \omega^2 \left(\frac{m^* \sigma_0}{Ne^2}\right)^2}$$

If normal incidence is assumed, the absorbtivity of a material can be calculated, again using Maxwell's equations and the appropriate boundary conditions. Figure 20 illustrates the geometry.

$$\bar{\nabla} \times \bar{E} = \hat{y} \frac{\partial E_x}{\partial z} = -\mu \frac{\partial H_y}{\partial t}$$

$$\bar{\nabla} \times \bar{H} = -\hat{x} \frac{\partial H_z}{\partial t} = \sigma E_x + \epsilon \frac{\partial E_x}{\partial t}$$

As before,

$$\bar{E} = E_0 \exp\{[-2\pi kz/\lambda] + [i\omega(t - nz/c)]\}$$

Substituting this expression for electric field into Maxwell's equations yields a relationship between \bar{H} and \bar{E} :

$$H_y = \left(\frac{n - ik}{\mu c}\right) E_x$$

The boundary conditions at the material interface are:

$$E_i + E_r = E_t$$

$$\mu_1 H_i - \mu_1 H_r = \mu_2 H_t$$

MEDIUM 1, VACUUM

MEDIUM 2, METALLIC SOLID

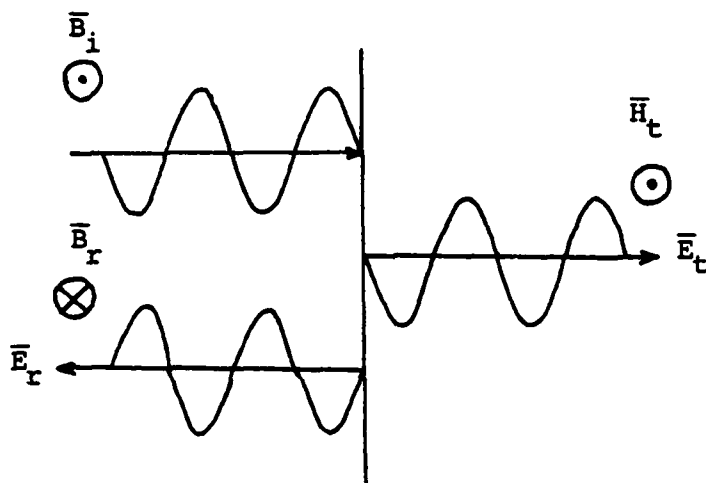


FIGURE 20. BOUNDARY CONDITIONS FOR \vec{E} AND \vec{B} FIELDS AT THE TARGET INTERFACE

The subscripts 1 and 2 are for the mediums. Medium 1 is vacuum and medium 2 is the target material. The subscripts i, r, and t denote incident, reflective and transmitted waves. Using these boundary conditions and the relationship for H_y in terms of E_x , the ratio of E_i/E_r can be readily obtained:

$$\frac{E_i}{E_r} = \frac{n-1-ik}{n-1+ik} = r$$

where r is the amplitude reflection coefficient. It has been assumed that $n_1 = 1$ and $k_1 = 0$, which is the case in vacuum. The reflectivity, R is given by $|r * r|$ and therefore is written as:

$$R = \frac{(n-1)^2 + k^2}{(n+1)^2 + k^2}$$

The absorbtivity, A , is the desired result of the derivation where:

$$A = (1 - R)$$

The abosrbtivity can be written as:

$$A = \frac{4n}{(n+1)^2 + k^2}$$

BIBLIOGRAPHY

1. Johnson, C. B., Induced Evaporation of Metal from an Aluminum Surface by a Normal Pulse Neodymium Laser, M. S. Thesis, U. S. Naval Postgraduate School, Monterey, CA, 1979.
2. Air Force Cambridge Research Laboratories Report 68, A Bibliography of the Electrically Exploded Conductor Phenomenon, W. G. Grace and E. M. Watson, 1967.
3. Colombant, D. G., Lampe, M., and Bloomberg, H. W., WHYRAC, A New Modular One-Dimensional Exploding Wire, NRL Memorandum, Report 3726, Naval Research Laboratory, Washington, D. C., 1978.
4. Brooks, K. M., An Investigation of Early Disturbances Found In Association With Laser-Produced Plasma, M. S. Thesis, U. S. Naval Postgraduate School, Monterey, CA, 1973.
5. Mott, N. F., and Jones, H., Properties of Metals and Alloys, Oxford University Press, London, pp. 105-114, 1936.
6. Fowles, G. R., Introduction to Modern Optics, Holt, Rinehart, and Winston, Inc., New York, pp. 160-164, 1968.
7. Weiting, T. J., and Schriempf, J. T., "Free-Electron Theory and Laser Interactions with Metals," Report of NRL Progress, pp. 1-13, Naval Research Laboratory, Washington, D. C., June 1972.
8. Seitz, F., Modern Theory of Solids, McGraw Hill Co., Inc., New York, New York, 1942.
9. Harrison, W. A., and Webb, M. B., The Fermi Surface, John Wiley and Sons, Inc., New York, New York, 1960.
10. Bennett, M., Silver, and Ashley, E. J., "Infrared Reflectance of Aluminum Evaporated in Ultra-High Vacuum," Journal of the Optical Society of America, vol. 53, no. 9, pp. 1089-1095.
11. CRC Handbook of Physics and Chemistry, 59th Edition, CRC Press, In., West Palm Beach, Florida, 1978.

12. Richmyer, F. K., Kennard, E. H., and Cooper, J. H., Introduction to Modern Physics, p. 598, McGraw-Hill Book Company, New York, 1969.
13. Bonch-Bruevich, A. M., et al., "Effect of a Laser Pulse on the Reflecting Power of a Metal," Soviet Physics-Technical Physics, vol. 13, no. 5, pp. 640-643, 1968.
14. Thomas, P. D., and Musal, H. M., Lockheed Report LSMC D352-890, 1973 (Unpublished).
15. Harrach, R. J., "Analytical Solution for the Laser Heating and Burnthrough of Opaque Solid Slabs," Journal of Applied Physics, vol. 48, no. 6, pp. 2370-2383, 1977.
16. Schriempf, J. T., Response of Materials to Laser Radiation: A Short Course, NRL Report 7728, Naval Research Laboratory, Washington, D. C., 1974.
17. Carslow, H. S. and Jaeger, J. C., Conduction of Heat in Solids, p. 58, Clarendon Press, Oxford, 1947.
18. Braginskii, V. B., Minakova, I. I., and Rudenko, V. N., "Mechanical Effects in the Interaction Between Pulsed Electromagnetic Radiation and a Metal," Soviet Physics-Technical Physics, vol. 12, no. 6, pp. 753-758, 1967.
19. Harrach, R. J., "Estimates on the Ignition of High-Explosives by Laser Pulses," Journal of Applied Physics, Vol. 47, no. 6, pp. 2473-2481, 1976.
20. Anisimov, S. I., "Evaporation of a Light-Absorbing Metal," High Temperature, vol. 6, pp. 110-114, 1968, Translated from Teplofizika Vysokikh Temperatur, vol. 6, no. 1, pp. 116-120, January-February 1968.
21. Kelley, K. K., "Contributions to the Data on Theoretical Metallurgy; XIII. High Temperature Heat Content, Heat Capacity and Energy Data for the Elements and Inorganic Compounds," Bureau of Mines Bulletin No. 584, U. S. Department of the Interior, Washington, D. C., 1960.
22. JANAF Thermochemical Tables, 2nd Edition, National Bureau of Standards, Washington, D. C., 1971.
23. Tanenbaum, H. M., Plasma Physics, pp. 8-12, McGraw Hill Book Company, New York, 1967.
24. Sargent-Welch Scientific Company, Table of Periodic Properties of the Elements, 1968.

INITIAL DISTRIBUTION LIST

	No. Copies
1. Defense Technical Information Center Cameron Station Alexandria, Virginia 22314	2
2. Library, Code 0142 Naval Postgraduate School Monterey, California 93940	2
3. Department Chairman, Code 61 Department of Physics and Chemistry Naval Postgraduate School Monterey, California 93940	2
4. Professor K. E. Woehler, Code 61Wh Department of Physics and Chemistry Naval Postgraduate School Monterey, California 93940	3
5. Associate Professor F. R. Schwirzke, Code 61Sw Department of Physics and Chemistry Naval Postgraduate School Monterey, California 93940	1
6. LT Geoffrey L. Travers, USN 222 Reamer Avenue Wilmington, Delaware 19804	1
7. Physics International 2700 Merced Street San Leandro, California 94577	1
8. Director Defense Nuclear Agency Washington, D. C. 20305	1